NASA TN D-484

*7N-17*
*199034*
*52ß*

# NASA

# TECHNICAL NOTE

D-484

# TELEMETRY CODE AND CALIBRATIONS FOR

# SATELLITE 1959 IOTA

# (EXPLORER VII)

Compiled and Edited by

I. L. Cherrick

NASA Headquarters Staff

## NATIONAL AERONAUTICS AND SPACE ADMINISTRATION

WASHINGTON                                            May 1960

# PREFACE

The establishment of a receiving station for the reception of the data from the satellite 1959 Iota (Explorer VII) is a reasonably modest undertaking, and the data are quite easily read and reduced to useable form. Interested groups are invited to make use of this instrumentation for their own investigations and to assist in expanding the coverage of the present network of receiving stations. Data from Central Africa, the Near and Far East, India, and the South Pacific are especially needed. Persons who obtain useable data and who wish to make it available to NASA are invited to send a list of their recordings specifying equipment used, date and time of recording, and data quality, to the following address:

> Assistant Director
> Satellite & Sounding Rocket Programs
> NASA Headquarters
> 1520 H Street, N. W.
> Washington 25, D. C.
> U. S. A.

This agency desires the loan of records for which we have no duplicate coverage. It is preferred that recordings sent to NASA be in the form of original magnetic tape recordings or tape copies of the original recordings. In the event that procurement of magnetic recording tape presents a problem, tapes sent to NASA will be returned after analysis if it is so requested.

Requests for the orbital elements of the ephemeris and/or the ephemeris printout should also be directed to the above address.

# CONTENTS

# LIST OF TABLES

# LIST OF FIGURES

# TELEMETRY CODE AND CALIBRATIONS FOR SATELLITE 1959 IOTA
## (EXPLORER VII)

## INTRODUCTION

Satellite 1959 Iota. a part of the United States participation in the International Geophysical Cooperation - 1959. was launched from Cape Canaveral, Florida, on 13 October 1959 at approximately 1530 universal time. The scientific payload (Figures 1 and 2), planned by the United States IGY Technical Panel on the Earth Satellite Programs, was designed to furnish data on: the radiation balance of the earth; solar Lyman-alpha and X-ray intensity; heavy primary cosmic ray intensity; total cosmic ray intensity; magnitude and time variations of the intensity of geomagnetically-trapped particles; solar protons; the performance of an unprotected solar cell; micrometeorite impacts; and the temperature at various points within the satellite. The telemetry for these experiments was divided between two radio transmitters. One transmitter. operating on 108 Mc and powered by mercury batteries, was used principally for tracking and the micrometeorite data. This transmitter has been inoperative since the batteries became exhausted on 5 December 1959. Another transmitter. operating on 19.992 Mc and powered by nickel-cadmium batteries that are charged from solar cells. continues to transmit data from the other experiments. Barring failure from other causes. this transmitter will operate until one year from the launch date. when an automatic timing device will cut off the power.

The numerous inquiries received by NASA indicate that many scientists around the world are interested in recording and analyzing the data from the 19.992-Mc transmitter. Therefore. in accordance with established NASA policy to cooperate with the international scientific community to the maximum extent feasible, the individual sponsors of the satellite experiments have made available for publication the complete telemetry codes and instructions for reducing the data. NASA has compiled and edited this information from the experimenters and the results are presented here.

Figure 1 - Components of 1959 Iota

COSMIC RAY DETECTOR

LYMAN ALPHA DETECTOR

HEAVY NUCLEI CHAMBER

20 MC ANTENNA RELEASE MOTOR

BATTERY BOX

108 MC ANTENNA (LOOP)

SEPARATION DEVICE

4TH STAGE

LONG DURATION TIMER

X-RAY DETECTOR

INSTRUMENT COMPARTMENT

20 MC ANTENNA SPOOL

MICRO-METEORITE EXPERIMENT

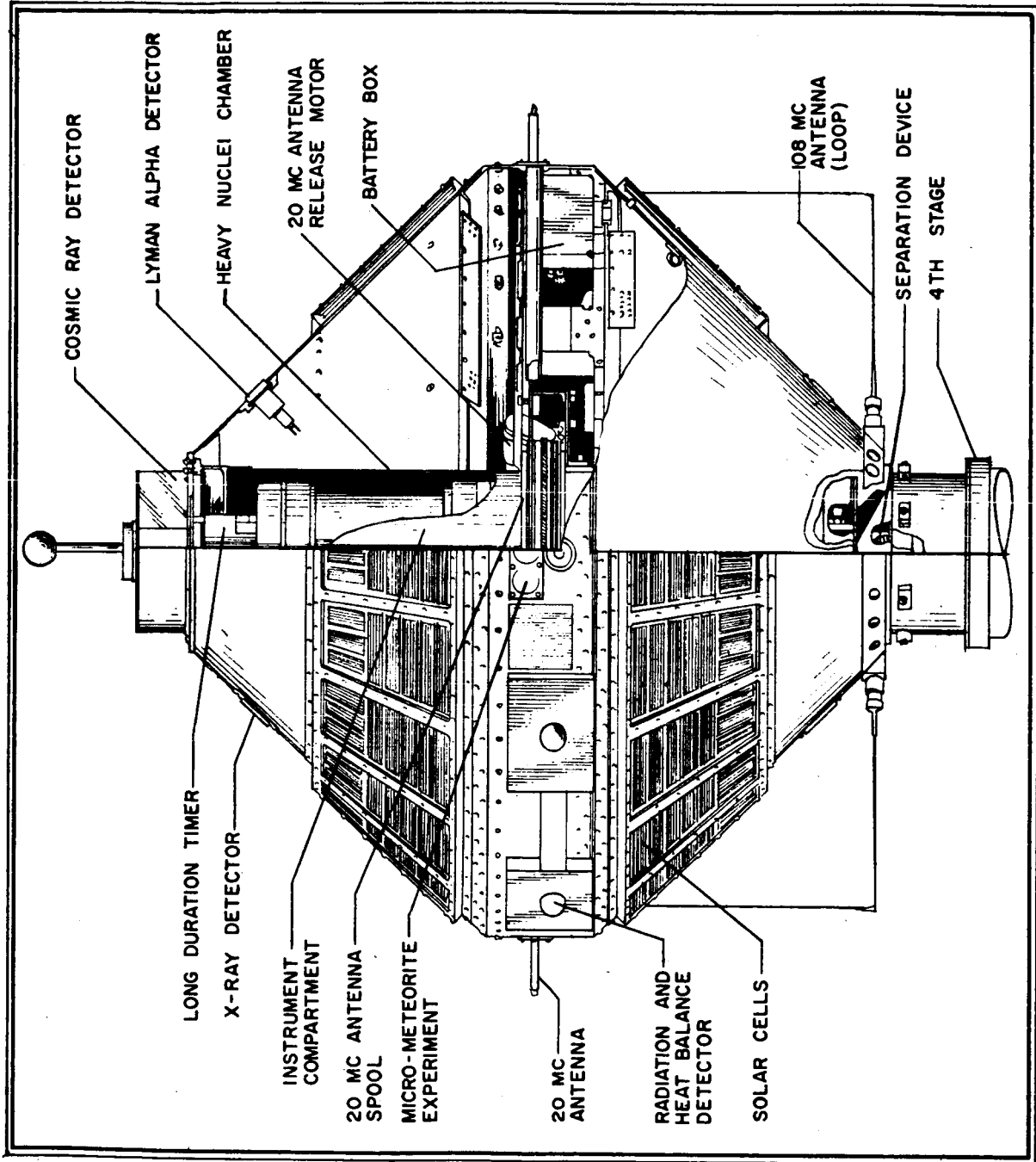20 MC ANTENNA

RADIATION AND HEAT BALANCE DETECTOR

SOLAR CELLS
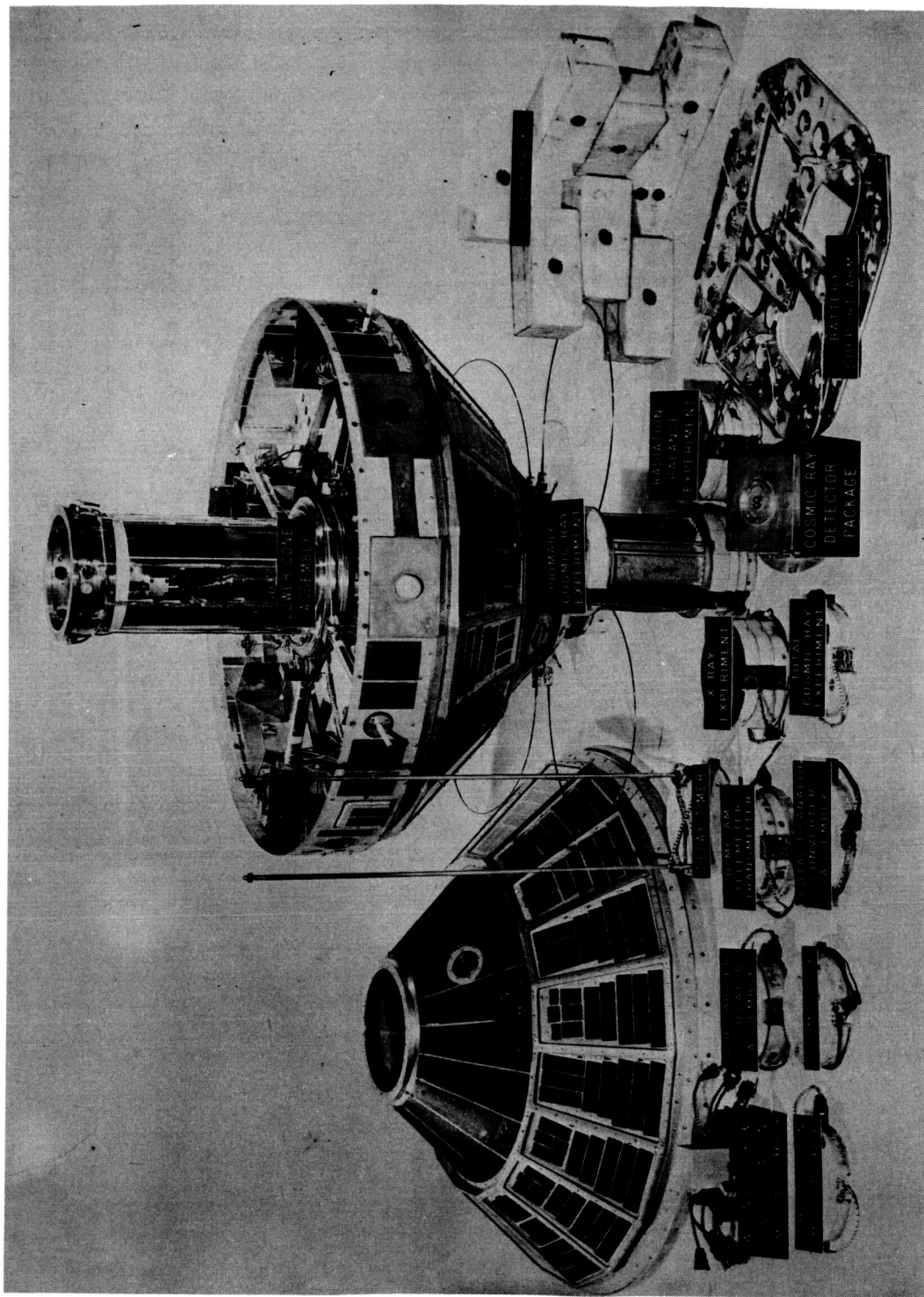
Figure 2 - Cutaway sketch of 1959 Iota

The material presented in this report is, in general, limited to that necessary to decode and convert to basic measurements the data transmitted on the 19.992-Mc telemetry signal. The interpretation of the results is discussed only insofar as the individual experimenters have supplied comments in this regard.

A complete listing of the measurements available from the 19.992-Mc telemetry system is given in Table 1 along with the names of the responsible individuals and agencies. The discussion relating to these measurements considers first a brief explanation of the satellite transmitter and the subcarrier modulation, and following this some suggestions relating to receiving and recording equipment necessary to obtain the basic telemetry records. The discussion relating to the reduction of the data from telemetered records to the measured quantities listed in Table 1 is, for convenience, organized under the headings of the various subcarrier frequencies.

# SATELLITE TRANSMITTER AND SUBCARRIERS

TRANSMITTER

The 19.992 Mc-transmitter has a power output of approximately 0.6 watt. The satellite antenna is a crossed dipole resulting in circular polarization when viewed end-on and linear polarization in the plane of the dipoles. The transmitted carrier is amplitude-modulated by the summed outputs of four frequency-modulated subcarriers. These FM subcarriers are United States standard audio frequency channels with a nominal maximum deviation of 7.5 percent and nominal center frequencies of 560, 730, 960, and 1300 cycles per second.

SUBCARRIER MODULATION

The types of modulation employed on the subcarriers are illustrated in Figure 3.

560-cps Subcarrier

The 560-cps subcarrier contains a twelve-bit clock pulse with one pulse missing for word reference. The pulses are 0.25 second in duration and the time between pulses is 0.25 second.

Table 1
Measurements transmitted on 19.992-Mc telemetry

| Measurement | Channel | Experimenter |
|---|---|---|
| Radiation Balance Experiment (Thermal) | 730 cps | Dr. Verner E. Suomi University of Wisconsin Madison, Wisconsin |
|   Hemisphere No. 1: Black; equally sensitive to solar and terrestrial radiation | | |
|   Hemisphere No. 2: White; more sensitive to terrestrial infrared radiation than solar | | " |
|   Hemisphere No. 3: has a sun shield | | " |
|   Hemisphere No. 4: same as Hemisphere No. 1 | | " |
|   Hemisphere No. 5: polished gold surface; more sensitive to direct solar radiation and earth albedo than to terrestrial infrared radiation | | " |
|   Sphere No. 6: Black; mounted on a post on the satellite axis (see Figure 2) | | " |
| Temperature | 730 cps | |
|   Mirror Temp. $M_1$ for Black Hemisphere No. 1 and the White Hemisphere | | Dr. Verner E. Suomi University of Wisconsin Madison, Wisconsin |
|   Mirror Temp. $M_2$ for Black Hemisphere No. 2 and the Gold Hemisphere | | " |
|   Skin Temperature | | George C. Marshall Space Flight Center (formerly ABMA) |
|   Solar Cell Tray Temperature | | " |
|   19.992-Mc Transmitter Base Plate Temperature | | " |
|   Battery Pack Temperature | | " |
|   Geiger-Mueller Counter Housing Temperature | | " |
| Lyman-alpha and X-ray Experiment | 960 cps | Dr. Herbert Friedman U.S. Naval Research Laboratory Washington, D.C. |
|   Detectors for Lyman-alpha Radiation | | |
|   Detectors for X-ray Radiation | | " |
| Solar Aspect | | " |

Table 1 (cont.)

| Measurement | Channel | Experimenter |
|---|---|---|
| Heavy Primary Cosmic Ray Experiment<br><br>Cosmic rays, Atomic Numbers $\geq 16$<br><br>Cosmic rays, Atomic Numbers $\geq 9$<br><br>Cosmic rays, Atomic Numbers $\geq 6$<br><br>Exposed Solar Cell<br><br>Solar Cells and Nickel-Cadmium Batteries (Power Supply Monitor) | 960 cps | Dr. Phillip Schwed; experiment developed by Dr. Gerhart K. Groetzinger, deceased, Research Institute for Advanced Studies (RIAS), Baltimore, Maryland<br><br><br>George C. Marshall Space Flight Center (formerly ABMA)<br><br>" |
| Total Cosmic Ray Experiment<br><br>Geiger-Mueller Counter (unshielded)<br><br>Geiger-Mueller Counter (shielded) | 1300 cps | Dr. James A. Van Allen, State University of Iowa (SUI) Iowa City, Iowa<br><br><br>" |

730-cps Subcarrier

The 730-cps subcarrier contains the data from the Radiation Balance Experiment in the form of a ten-bit natural binary-coded word. The pulses are synchronous with the 560-cps channel "sprocket" pulses and have the same width and spacing. The ten-bit word is sent with the least significant digit first, coincident with the first sprocket pulse following the missing pulse. The eleventh sprocket pulse position is not used and has no value. A complete data frame, 378 seconds long, is made up of nine subframes; each subframe is 42 seconds long and contains seven ten-bit binary words, each 6 seconds in length, for a total of 63 ten-bit words (Table 2).

960-cps Subcarrier

The data on the 960-cps subcarrier are commutated every 1.5 seconds. Each frame is 15 seconds in length and contains the following ten measurements in the order indicated: (1) 5.5-volt Reference; (2) 0-volt Reference; (3) Lyman-alpha and X-ray; (4) Cosmic-Ray Particles, Atomic No. $\geq 16$; (5) repetition of Lyman-alpha and X-ray; (6) Cosmic-Ray Particles, Atomic No. $\geq 9$; (7) Solar Aspect; (8) Cosmic-Ray Particles,
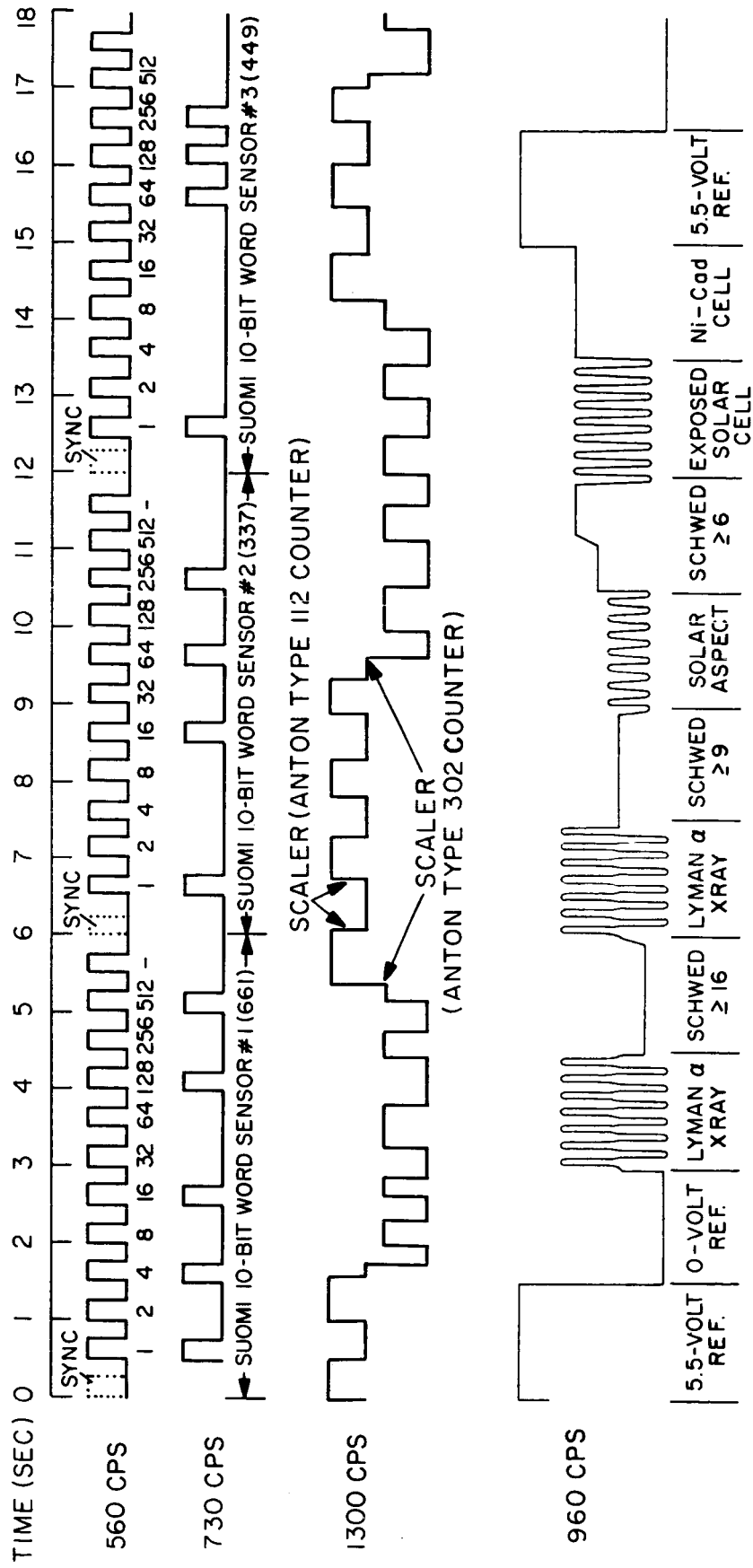
Figure 3 – Ideal sketch of a typical demodulated record

Table 2
Sampling order for the 730-cps subcarrier

| Word Sequence | (1) | (2) | (3) | (4) | (5) | (6) | (7) |
|---|---|---|---|---|---|---|---|
| (1) | $B_1$ | $W_2$ | $T_3$ | $B_4$ | $G_5$ | $B_6$ | Low Reference (64-65) |
| (2) | $B_1$ | $W_2$ | $T_3$ | $B_4$ | $G_5$ | $B_6$ | High Reference (985 - 999) |
| (3) | $B_1$ | $W_2$ | $T_3$ | $B_4$ | $G_5$ | $B_6$ | Skin Temperature |
| (4) | $B_1$ | $W_2$ | $T_3$ | $B_4$ | $G_5$ | $B_6$ | Solar Cell Temperature |
| (5) | $B_1$ | $W_2$ | $T_3$ | $B_4$ | $G_5$ | $B_6$ | Transmitter Temperature |
| (6) | $B_1$ | $W_2$ | $T_3$ | $B_4$ | $G_5$ | $B_6$ | Battery Temperature |
| (7) | $B_1$ | $W_2$ | $T_3$ | $B_4$ | $G_5$ | $B_6$ | Geiger-Mueller Tube Temperature |
| (8) | $B_1$ | $W_2$ | $T_3$ | $B_4$ | $G_5$ | $B_6$ | Mirror ($M_1$) Temperature for $B_1$, $W_2$ |
| (9) | $B_1$ | $W_2$ | $T_3$ | $B_4$ | $G_5$ | $B_6$ | Mirror ($M_2$) Temperature for $B_4$, $G_5$ |

Complete Set, 378 Seconds

| (1) | $B_1$ | $W_2$ | $T_3$ | $B_4$ | $G_5$ | $B_6$ | Low Reference |
|---|---|---|---|---|---|---|---|
| (2) | | | | | | | |
| (3) | | | | | | | |

Word 6 seconds        Etc.

Complete sequence, 42 seconds

| Word | | Word | | Word | |
|---|---|---|---|---|---|
| 1 | Black Hemisphere No. 1 ($B_1$) | 4 | Black Hemisphere No. 2 ($B_4$) | 7 | Auxiliary Data |
| 2 | White Hemisphere ($W_2$) | 5 | Gold Hemisphere ($G_5$) | | |
| 3 | Shaded Hemisphere ($T_3$) | 6 | Black Sphere ($B_6$) | | |

Atomic No. ≳ 6; (9) Exposed Solar Cell; (10) Nickel-Cadmium Battery and Solar-Cell Voltage (supply for multiplexer and voltage converter).

## 1300-cps Subcarrier

The 1300-cps subcarrier contains data from the two Geiger-Mueller counters used in the cosmic-ray experiment modulated as a four-step frequency shift. The analog output resembles a small square wave with a high repetition rate, modulated by a larger square wave with a lower repetition rate. The repetition rate of the small deviation as shown in Figure 3 is the scaled counting rate of the Anton 112 Geiger-Mueller counter.

The repetition rate of the larger deviation is the scaled counting rate of the Anton type 302 Geiger-Mueller counter.

# GROUND EQUIPMENT

### RECEIVING EQUIPMENT

Useable signals can be received from the satellite with very modest equipment. Simple half-wave dipoles mounted in quadrature and either selected for optimum performance or connected for circular polarization can be used for an antenna. Any low-noise AM (amplitude-modulated) receiver capable of tuning to 19.992 Mc and having a passband of at least 3 kilocycles may be satisfactory; however, greater success may be obtained if the receiver has very steep cutoff characteristics outside the passband. The spectrum is very crowded near this frequency and high selectivity is needed to separate the signal from the interference.

### RECORDING AND TIMING EQUIPMENT

The receiver output can be connected directly to filter-discriminators tuned to the subcarrier frequencies, and the resulting discriminator outputs can be connected directly to a suitable paper recorder to obtain a demodulated record in real time. However, the preferred method is to record the signals on magnetic tape by means of at least a two-channel recorder of instrumentation quality. The satellite signal should be recorded on one channel and a timing signal, at least once every second, on the other. Because of the importance of time in correlating received data with the satellite position, the timing signal should be synchronized with WWV (broadcasting time signals from the United States) or an equivalent standard, and should preferably contain a 1-Kc timing wave. It is suggested, in addition to the recording of an accurate time signal, that a log be kept for each reel of tape. For each pass recorded the log should indicate the universal time when the recorder is started and stopped, and any pertinent comments about reception.

If the data are recorded on magnetic tapes, any number of analog records of the demodulated subcarriers can be obtained at the operator's convenience by connecting the output of the tape recorder to the input of a filter-discriminator tuned to the desired subcarrier frequency. The outputs from the discriminator and from the timing channel

of the tape recorder can then be connected to a suitable paper recorder with a pen response of at least 30 cps and paper speeds of the order of 2.5 cm/sec.

A reproduction of an actual demodulated record, made from a magnetic tape recording of a received signal from the 19.992-Mc transmitter, is shown in Figure 4.

# EXPERIMENT CALIBRATIONS AND DECODING PROCEDURES

560-CPS AND 730-CPS SUBCARRIERS

General

The data for the thermal radiation experiment and the other temperature measurements are telemetered on the 560-cps and the 730-cps subcarriers, respectively.

Radiation Balance Experiment

The purpose of this experiment is to measure the thermal radiation budget of the earth. This budget is determined by the amount of direct sunlight incident on the "top" of the atmosphere; the fraction of this sunlight that is reflected by the earth's surface, clouds, and atmosphere and does not enter into the thermodynamic system; and the "terrestrial" radiation lost from the earth and atmosphere by virtue of its absolute temperature. The net radiation received by the earth's surface is a function of latitude, time of year, time of day, and the structure of the atmosphere. The weather affects the net radiation received, and at the same time the unequal distribution of this net radiation over the earth's surface is the basic source of the world's weather.

The thermal radiation sensors on board 1959 Iota are simple omnidirectional bolometers. There are four unshaded hollow hemispherical shells, 3.25 cm in diameter, of thin sheet silver. They are mounted upon but thermally isolated from four rectangular aluminized mirrors located on the satellite equator (Figures 1 and 2, and Table 3). The dimensions of the hemispheres and the mirrors are such that no hemisphere "sees" any other hemisphere, other mirror, or any part of the satellite except the antenna wires. It is easily shown that, so long as the satellite is spinning, and except for reflection and heat conduction losses, each hemisphere is equivalent to an isolated sphere in space. With knowledge of the surface properties of each hemisphere, its heat capacity, and its conduction losses
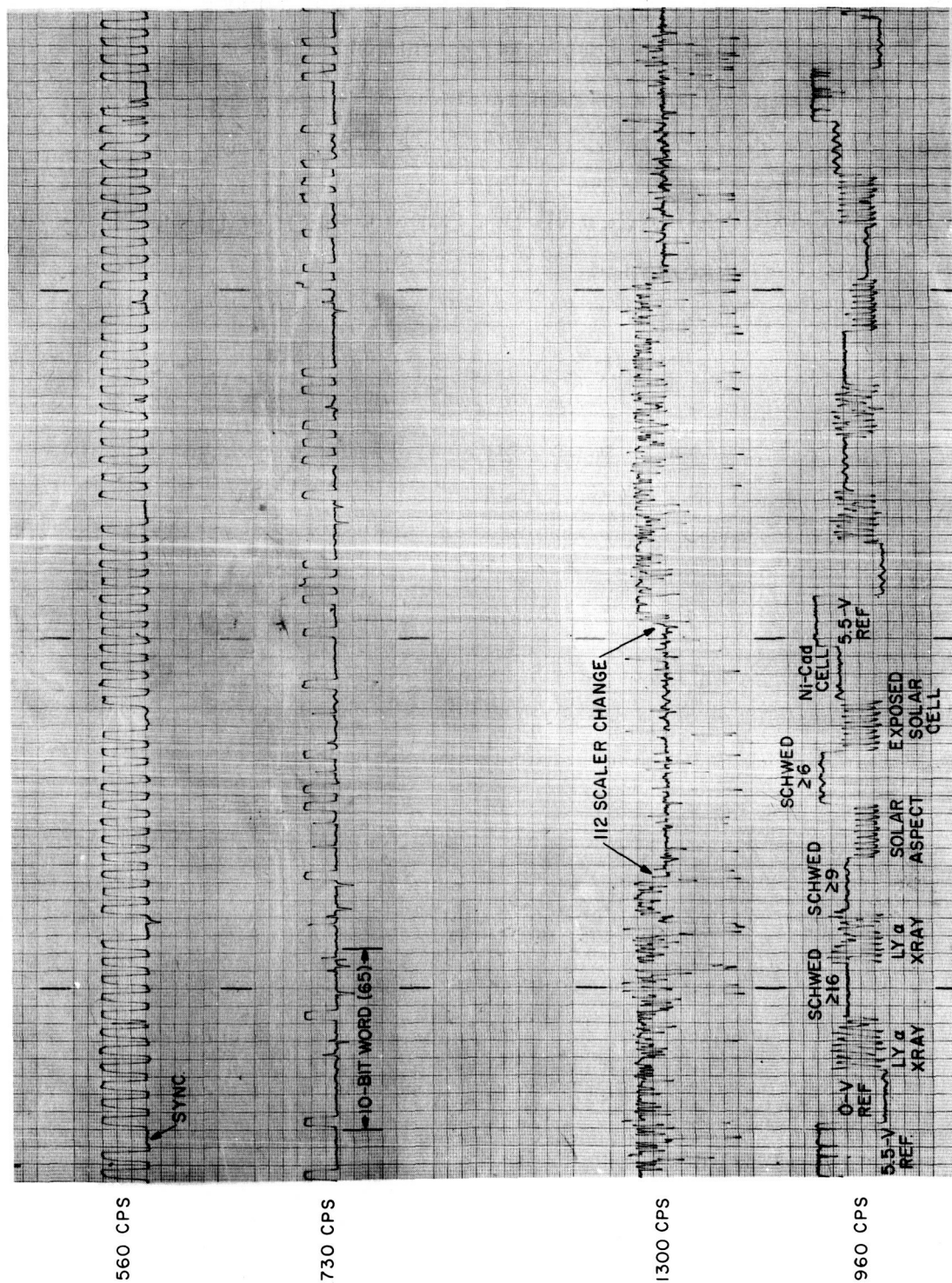
Figure 4 -- Annotated actual demodulated record

through its mounting (Table 3), the heat balance of each hemisphere may be calculated

from its temperature. This temperature, measured with a thermistor, is the information

telemetered to earth. The heat balance of each hemisphere is determined by the radia-

tions from the sun and the earth, i.e., the objects of the experiment. Two of the hemi-

spheres are black and are about equally sensitive to solar and terrestrial radiations.

Another is painted white and is more sensitive to terrestrial infrared radiation than to

direct or earth-reflected solar. (There is, however, more solar radiation.) The fourth

hemisphere has a polished gold surface which makes it more sensitive to direct or earth-

reflected solar radiation than to terrestrial infrared. Finally, there is a black sphere

mounted on a post on the satellite axis and a sensor with sun shield (shaded hemisphere)

mounted on a mirror on the equator. Details on the parameters of the six sensors are

given in Table 3.

Table 3
Sensor parameters for the Radiation Balance Experiment

| Sensor | $\alpha$ | $\epsilon$ | K | H |
|---|---|---|---|---|
| Black Hemisphere No. 1 | .91 | .91 | .004* | .0085 |
| White Hemisphere | .20 (est.) | .93 | .004 | .0083 |
| Shaded Hemisphere | .77 | .28 | .012** | unknown |
| Black Hemisphere No. 2 | .91 | .91 | .004 | .00847 |
| Gold Hemisphere | .34 | .04 | .004 | .0088 |
| Black Sphere | .91 | .91 | .003 | .00885 |

$\alpha$ - Absorbtivity of solar radiation (approximately 0.3 to 3 $\mu$).

$\epsilon$ - Emissivity for long wave radiation (approximately 3 to 60 $\mu$).

K - Conduction per $cm^2$ of surface per °C of temperature differ-
ence between sensor and mount.

H - Heat capacity, calories per $cm^2$ of exposed surface per °C.

*Measured at -50°C
**Calculated

## Temperature Experiment

Temperature measurements are made within the satellite to furnish auxiliary data required in evaluating the performance of the payload instrumentation and the adequacy of the satellite engineering with regard to heat balance. Temperatures are measured in the following locations: (1) the satellite skin; (2) a solar cell panel on the lower half of the satellite; (3) the 19.992-Mc transmitter base plate; (4) a nickel-cadmium battery pack; and (5) the top of the Geiger-Mueller counter housing.

## Telemetry Code and Calibrations

The subcarriers are shifted from their lowest values, 0.94 × 560 cps and 0.94 × 730 cps, to their highest values, 1.06 × 560 cps and 1.06 × 730 cps, by a pulse-code modulation system. The coding system converts each sensor temperature into a ten-digit binary number, called the "sensor count." These "sensor counts" are transmitted on the 730-cps subcarrier. The beginning and the ending of each ten-digit binary number is indicated by the distinctive pattern on the 560-cps subcarrier channel, called the sprocket.

The 560-cps sprocket channel transmission consists of eleven consecutive tone changes of 0.25-second duration at a rate of two per second; a pause corresponding to the twelfth position; and then a repetition of the cycle. The pause marks the beginning of each new ten-digit binary number. Thus, in order to decode the data the 560-cps sprocket subcarrier channel and the 730-cps subcarrier must be used together. The sprocket marks the beginnings and the endings of numbers, and the digit positions. The 730-cps signal marks the ones and zeros of the binary numbers. The least significant digit is received first, i.e., position 1 has the value 1, position 2 the value 2, position 3 the value 4, position 4 the value 8, and so on to position 10 with the value 512. Position 11 has no value.

The above procedure for decoding each number is illustrated in Figure 3. For example, the first ten-bit word in the illustration has a value of 661, obtained by summing the indicated values of the pulses, i.e., 1 + 4 + 16 + 128 + 512 = 661.

The maximum value of the ten-digit binary number is 1023, or $2^{10}$ - 1. When the white sensor $W_2$ is in full sunlight its temperature is high enough to cause the digital

converters to recycle the binary counter. Under these circumstances one must add 1024 to the decoded number to obtain the correct value. This is easily recognized as a large discontinuity in the count with time which disappears if 1024 is added. When the satellite is in the earth's shadow the black and gold sensors cool enough to be out of range; the numbers transmitted are then zeros. The white and shaded sensor temperatures however, together with the auxiliary temperatures, will still be within the calibrated range.

The data are transmitted as a sequence of seven numbers corresponding in order to the first black hemisphere $B_1$, white hemisphere $W_2$, shaded hemisphere $T_3$, second black hemisphere $B_4$, gold hemisphere $G_5$, black sphere $B_6$, and auxiliary data. There are transmitted a total of nine sequences to complete a set of data.

Each number, including the blank positions, takes 6 seconds; each sequence requires 42 seconds and the entire set requires 378 seconds or 6.3 minutes; then the cycle repeats. Table 2 gives the order for this entire cycle.

The keys to the identification of the various measurements are the low and high reference, transmitted as the seventh number of the first and second sequences respectively. The binary equivalent of the decimal number 64 or 65 is transmitted as the low reference, while a binary equivalent of the decimal number from 985 to 999 is transmitted as the high reference. The lack of constancy as to the exact value of the references has not been found to be a serious problem. It is due to the temperature sensitivity of the resistors in the binary scaling circuits.

After each word has been identified with a particular sensor and the value of the corresponding ten-bit binary number is determined, the sensor temperatures can be obtained from the calibration curves shown in Figures 5A through 5D. Alternatively, more accurate values of the sensor temperatures than can be obtained from the curves in Figures 5A, 5B, and 5C, may be calculated from the equations and constants listed in Table 4. These equations are not valid over the entire temperature range shown in the calibration curves, but they are valid over the range of temperatures experienced by 1959 Iota.
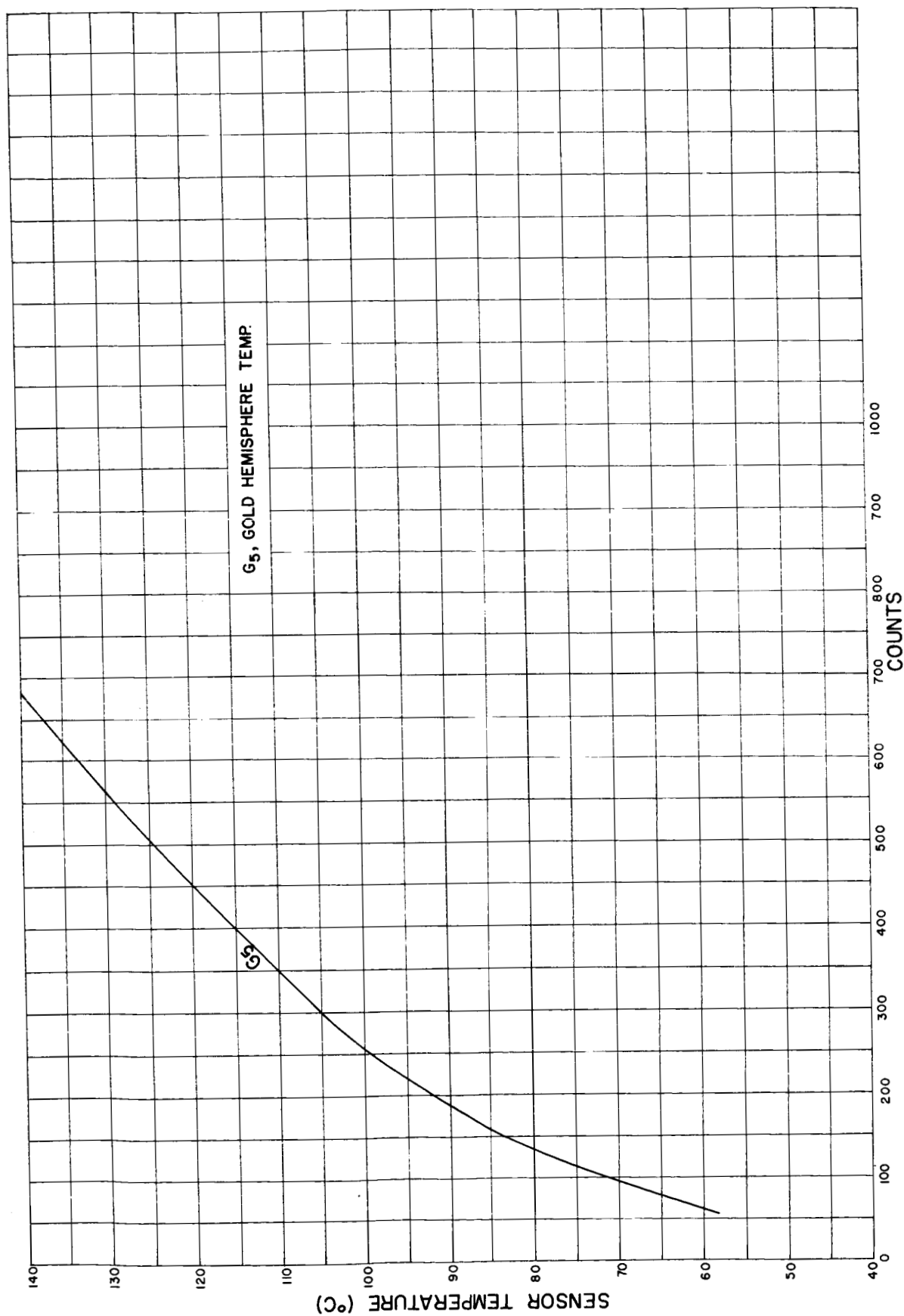
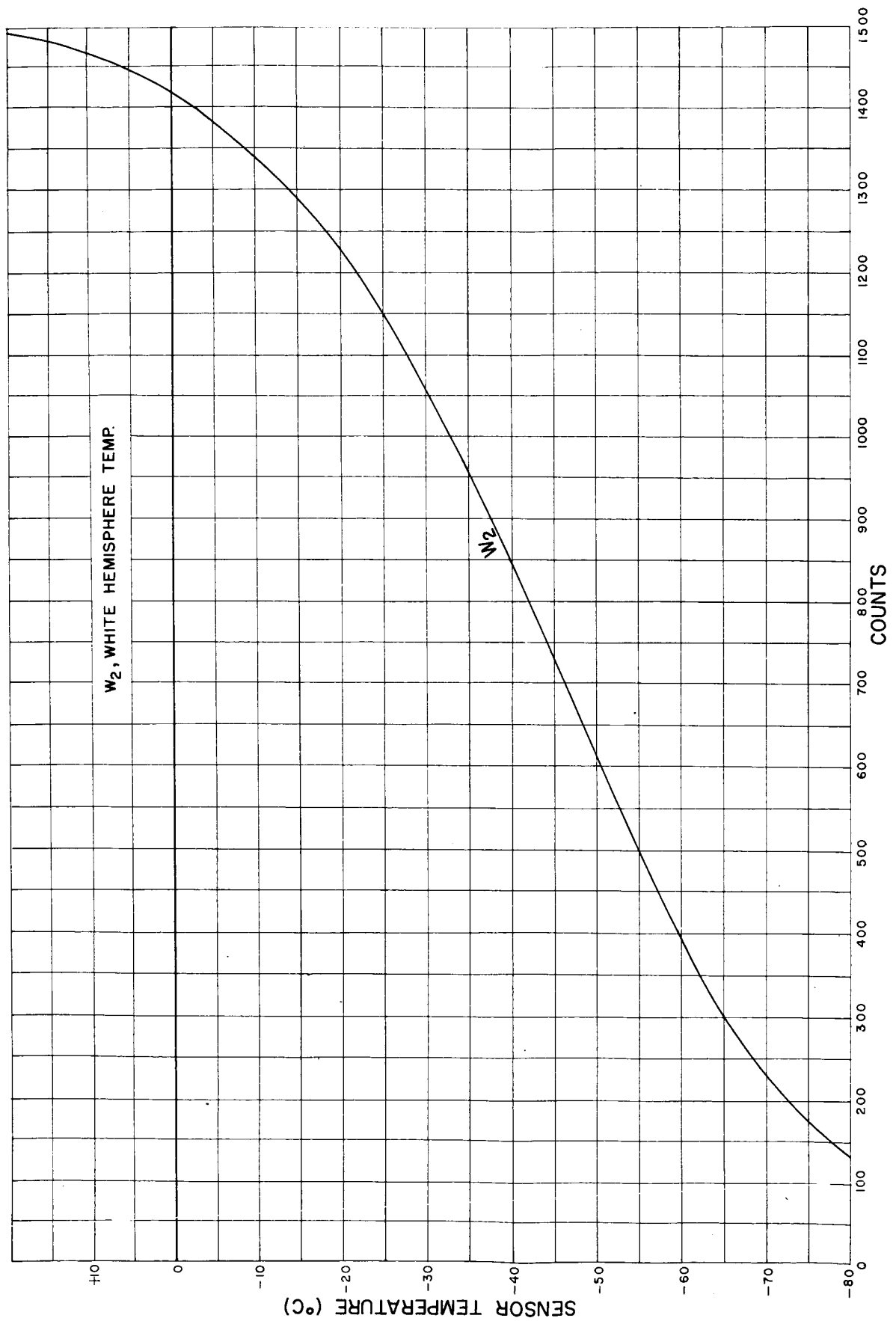Figure 5A - Calibration curves for the 730-cps subcarrier; temperature as a function of telemetered counts

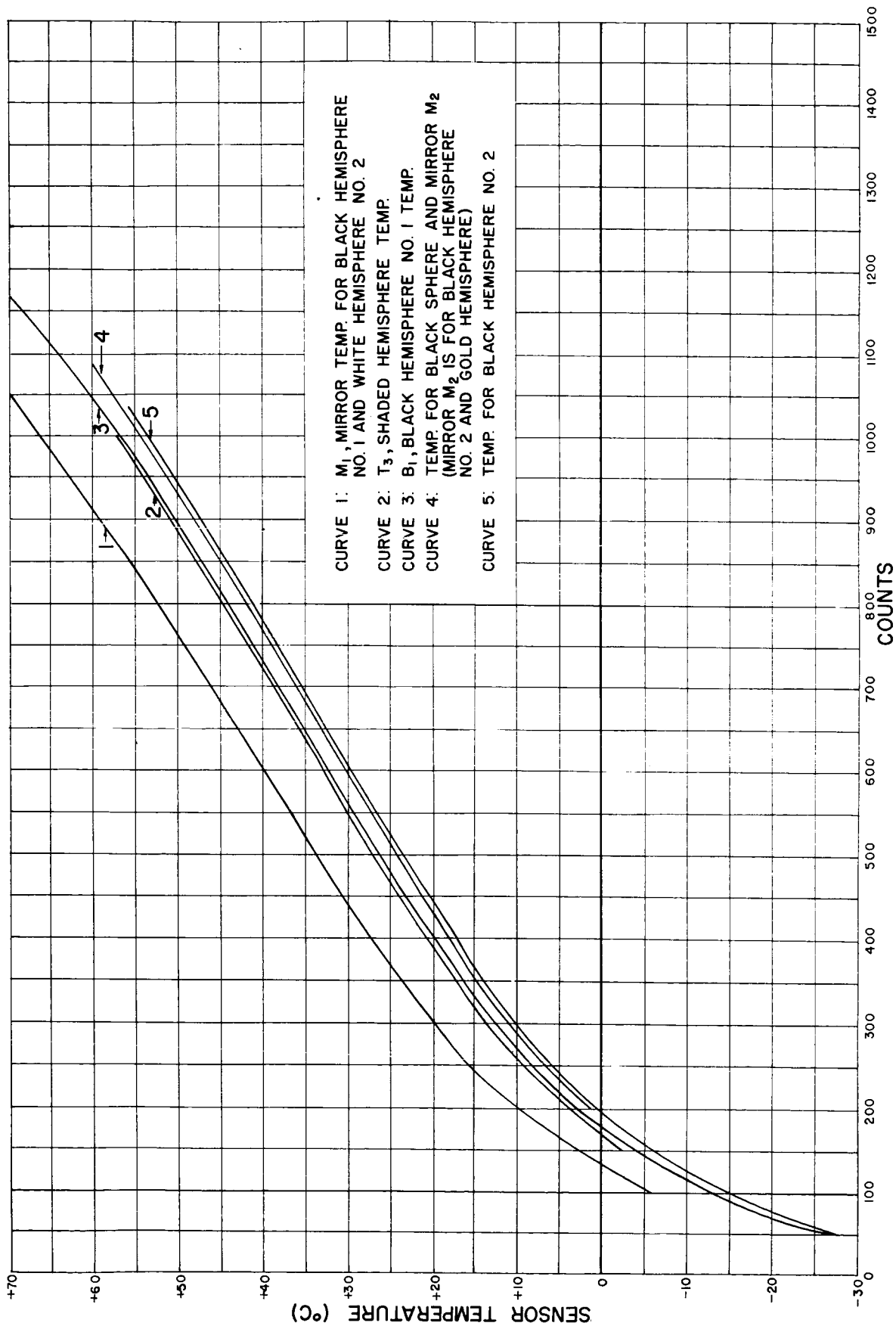Figure 5B - Calibration curves for the 730-cps subcarrier; temperature as a function of telemetered counts

Figure 5C - Calibration curves for the 730-cps subcarrier; temperature as a function of telemetered counts

CURVE 1: M₁, MIRROR TEMP. FOR BLACK HEMISPHERE NO. I AND WHITE HEMISPHERE NO. 2

CURVE 2: T₃, SHADED HEMISPHERE TEMP.

CURVE 3: B₁, BLACK HEMISPHERE NO. I TEMP.

CURVE 4: TEMP. FOR BLACK SPHERE AND MIRROR M₂ (MIRROR M₂ IS FOR BLACK HEMISPHERE NO. 2 AND GOLD HEMISPHERE)

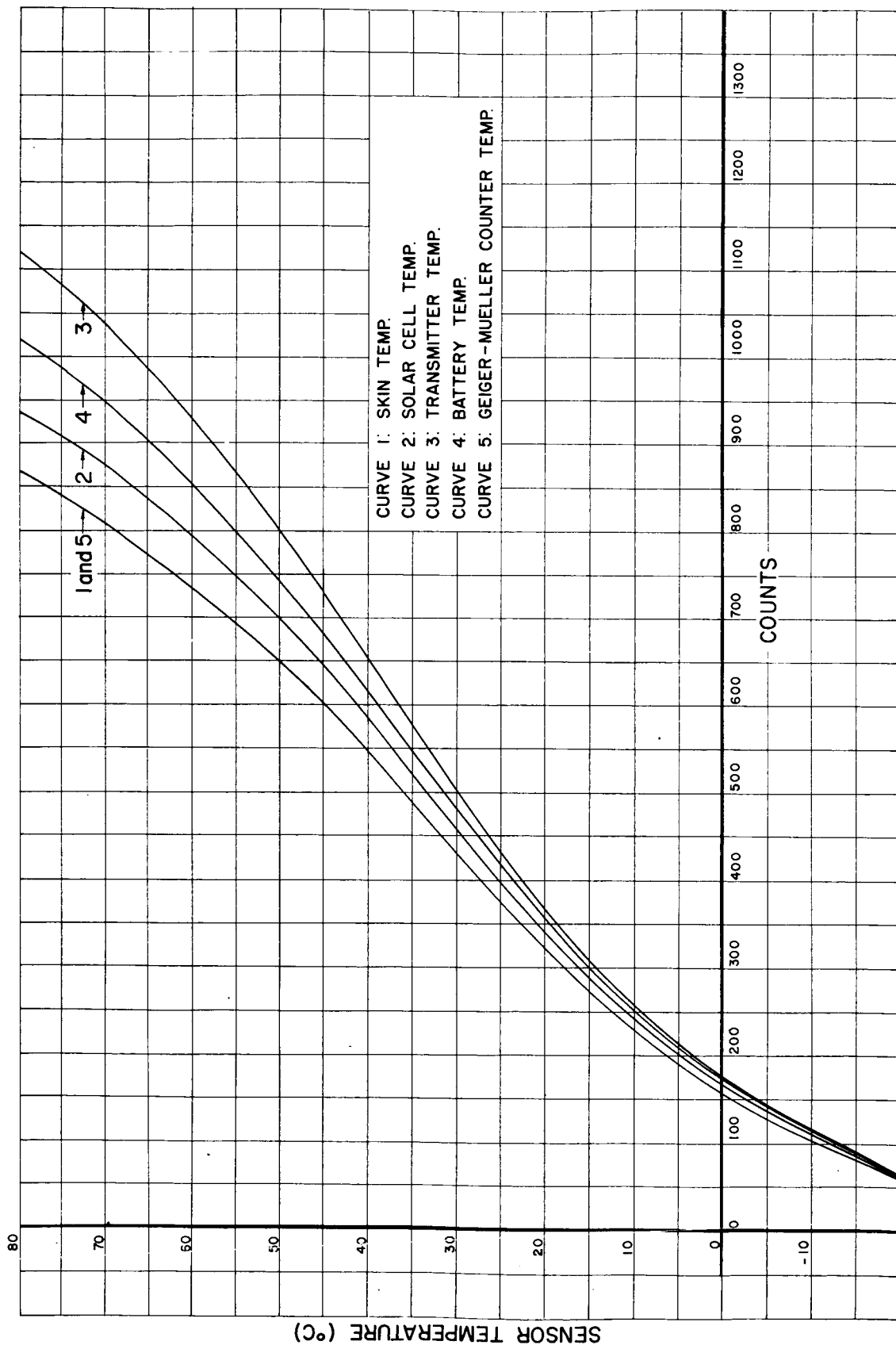CURVE 5: TEMP. FOR BLACK HEMISPHERE NO. 2

Figure 5D - Calibration curves for the 730-cps subcarrier; temperature as a function of telemetered counts

Table 4
Equations and constants for sensor calibrations

| | | | | | |
|---|---|---|---|---|---|
| $T = A_o + A_1X + A_2X^2 + A_3X^3 + A_4X^4$ | | | | | |
| $T$ = Temperature in degrees C | | | | | |
| $X$ = Counts received times $10^{-2}$ | | | | | |
| $A_o$ thru $A_4$ are constants and are listed below for each sensor: | | | | | |

| Sensor* | $A_o$ | $A_1$ | $A_2$ | $A_3$ | $A_4$ |
|---|---|---|---|---|---|
| $M_1$ | -47.587751 | +90.019611 | -72.101938 | +30.618146 | -4.875383 |
| $M_2$ | -31.322608 | +24.066135 | - 4.828245 | + 0.585730 | -0.02707547 |
| $B_1$ | -37.208385 | +33.086717 | - 8.2964098 | + 1.130905 | -0.057147924 |
| $W_2$ | -97.498257 | +15.503740 | - 1.9226768 | + 0.11380204 | +0.0014661498 |
| $T_3$ | -38.761168 | +40.928388 | -14.794268 | + 3.1504303 | -0.26977554 |
| $B_4$ | -38.991704 | +32.725429 | - 8.4489811 | + 1.2148790 | -0.066019706 |
| $G_5$ | +34.463138 | +51.257195 | -16.898667 | + 3.3762514 | -0.27452742 |
| $B_6$ | -31.322608 | +24.066135 | - 4.8282449 | + 0.58572993 | -0.027075468 |

*Sensors are defined in Table 2.

## 960-CPS SUBCARRIER

### General

An examination of Figure 3 will reveal the data contained on the 960-cps subcarrier. Briefly, the channel is commutated into segments 1.5 seconds in length in the repetitive sequence 15 seconds in length as shown in Figure 3. At the beginning of each sequence are high (5.5-volt) and low (0-volt) references to which displacements of the quantities in the other data frames are to be related. The measured displacements of the other signals are expressed as values of voltage from 0 to 5.5 volts, by a linear interpolation of the displacements between the reference signals. These voltages then related to the desired data, e.g., Lyman-alpha intensity, through the calibration curves presented in a subsequent section of this report.

## Lyman-alpha, X-ray, and Solar Aspect

### General

As is indicated in Figure 3, the Lyman-alpha and X-ray experiments are both recorded on the same segments of the sequence, numbers 3 and 5. The solar aspect is recorded on segment 7. Since the data from this measurement (the direction of the sun relative to the Lyman-alpha and X-ray detectors) are used in arriving at the results of the Lyman-alpha and X-ray experiments, the three measurements and their interpretations will be discussed together.

Solar Lyman-alpha and X-rays are each measured by means of coupled ionization chambers: two for Lyman-alpha and two for X-rays. The solar aspect is measured by means of a vacuum photocell with a restricted aperture. Figure 6 illustrates the relative placement on the satellite of the ionization chambers and the photocell.

### Lyman-alpha sensors

The Lyman-alpha ionization chambers are cylindrical in shape, 1.9 cm in diameter, and 3.2 cm long. They are fitted with a lithium fluoride window with an exposed effective aperture of $6.131 \times 10^{-4}$ cm$^2$ and are filled with nitric oxide (NO) at a pressure of 15 mm of mercury. The complete detectors have a quantum yield of 29 percent and are sensitive to wavelengths between 1040A, as determined by the transparency of the lithium fluoride window, and 1340A, as determined by the ionization potential of the nitric oxide gas.

### X-ray sensors

The X-ray sensors are similar to the Lyman-alpha sensors except for the filling gas and window material. The maximum quantum efficiency is calculated to be 77 percent and occurs at 2.8A. The spectral response curve is shown in Figure 7. The main structural features of the X-ray detectors are as follows:

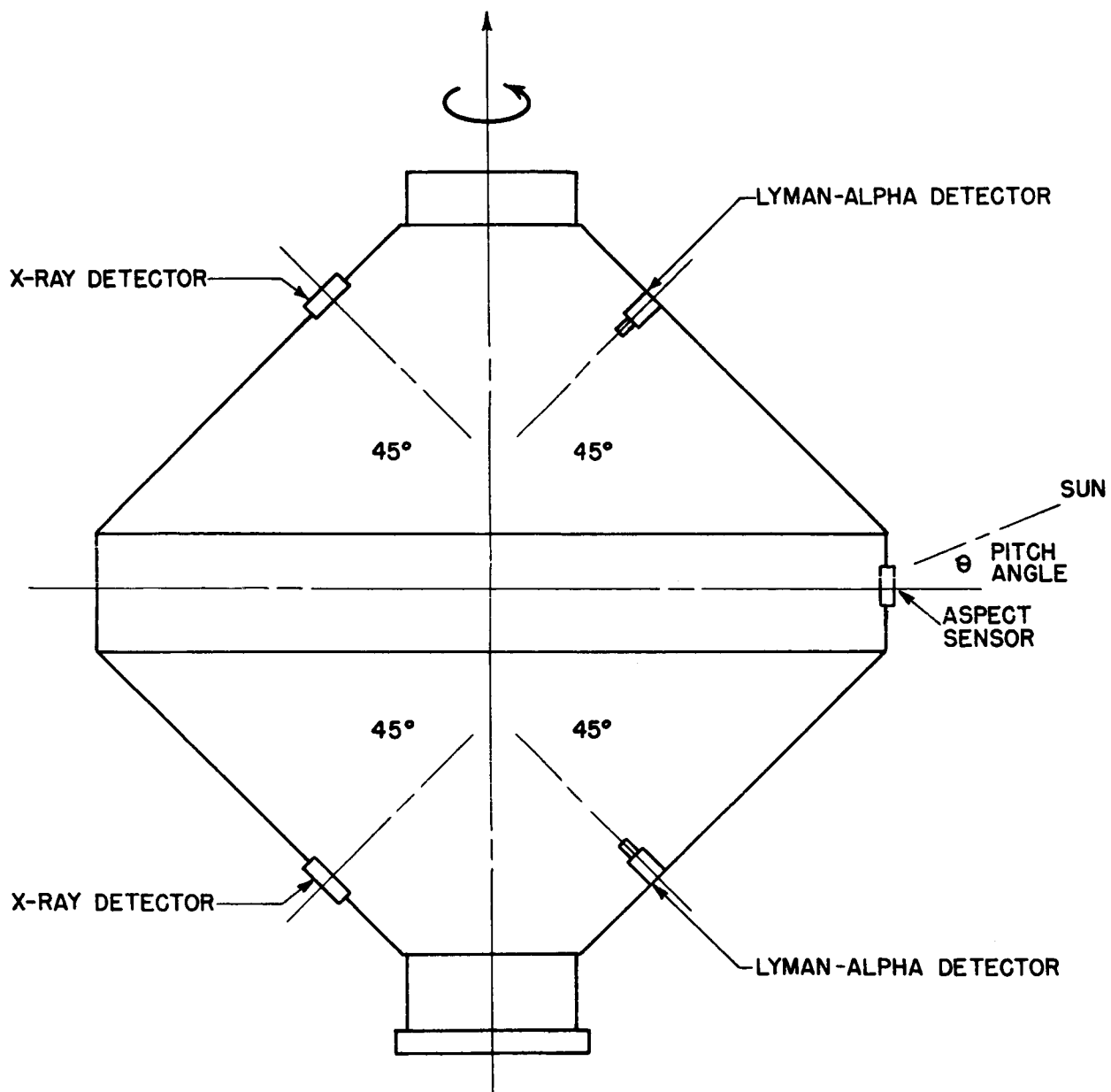| | |
|---|---|
| Window material: | Beryllium metal |
| Window surface density: | 0.021 gm/cm$^2$ |
| Window open area: | 6.83 cm$^2$ |
| Absorbing gas: | Argon |
| Pressure NTP: | 692 mm Hg |
| Depth at normal incidence: | 2.54 cm |

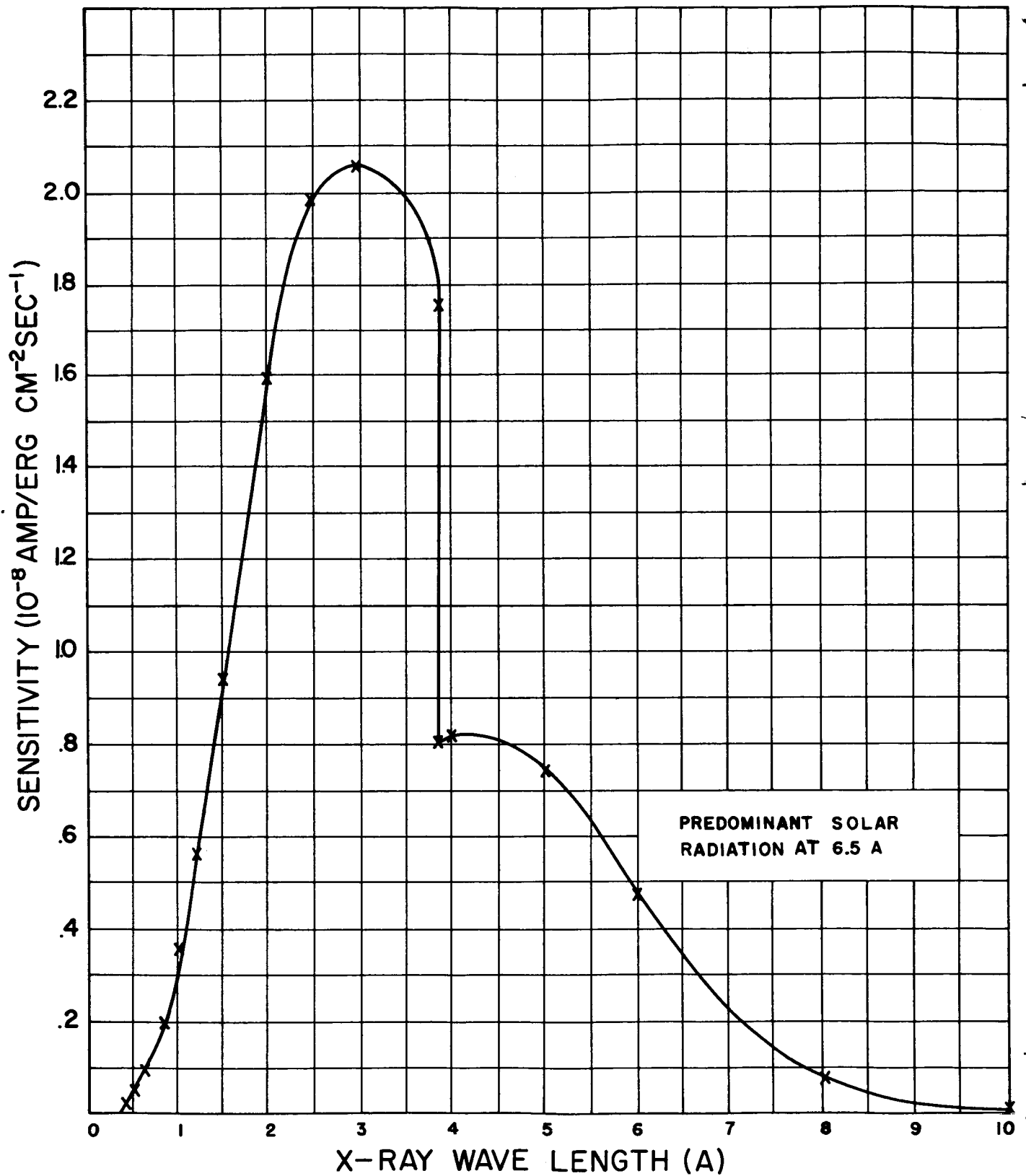Figure 6 - Locations of the Lyman-alpha, X-ray,
and solar aspect sensors

Figure 7 - Sensitivity of the X-ray detector at 45-degree aspect angle

The X-ray sensors are also sensitive to both gamma rays and electrons. Figure 8 shows a calibration of this sensitivity to gamma rays as determined from the gamma radiation of a cobalt-60 source. A similar calibration of the relation between electron energy and sensor current is not available. However, the X-ray ion chambers are known to respond to electrons of energy greater than 150 kev.

*Data reduction*

Since the Lyman-alpha and X-ray data are both contained on the same segments, 3 and 5, of the 960-cps subcarrier, the first step in the data reduction is to measure the deflections of the peaks of the waveforms. The Lyman-alpha data will be obtained from the voltage reading of the negative peaks (negative relative to the segment zero reference, about 2.05 volts above system zero reference), and the X-ray data will be obtained from the voltage reading of positive peaks. The values of voltage can be obtained from the measured deflections and the 0-volt and 5.5-volt reference measurements. Values of the ionization current can then be obtained from the calibration curves of Figure 9.

The next step in the data reduction is to obtain values of the solar aspect correction factor based on the following considerations. Since the satellite presumably spins about an axis perpendicular to that of the photocell and located in a plane containing the photocell and the Lyman-alpha and X-ray sensors (see Figure 6), a measurement of the maximum output of the sensor can be used to estimate the angle between the axis of the ion chamber and the direction of the sun. A measurement of the number of cycles per second will be equivalent to the spin rate. The measurements of the maximum output of the sensor, converted to volts by referring back to the 0-volt and the 5.5-volt reference, are used along with Figure 10 to estimate the pitch angle.

The final step in the reduction of the X-ray data is to take the X-ray sensor current (Figure 9) and obtain the correction factor for pitch angle by using Figures 10 and 11A. The corrected detector current is then divided by the sensitivity factor taken from Figure 7 (the predominant solar radiation response occurs at 6.5A) to obtain the incident X-ray flux in ergs/cm$^2$/sec.
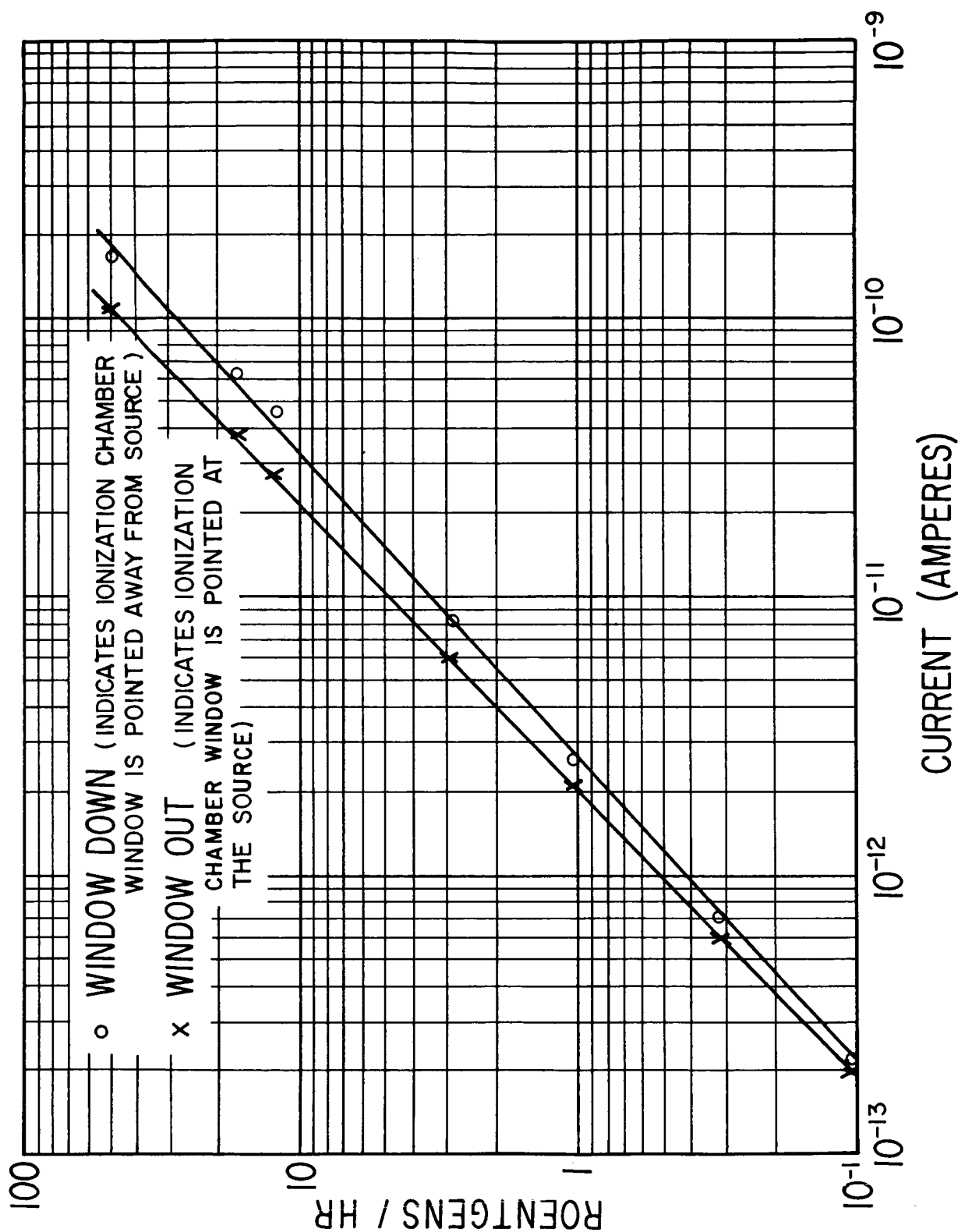
Figure 8 - Sensitivity of the X-ray sensors to gamma radiation
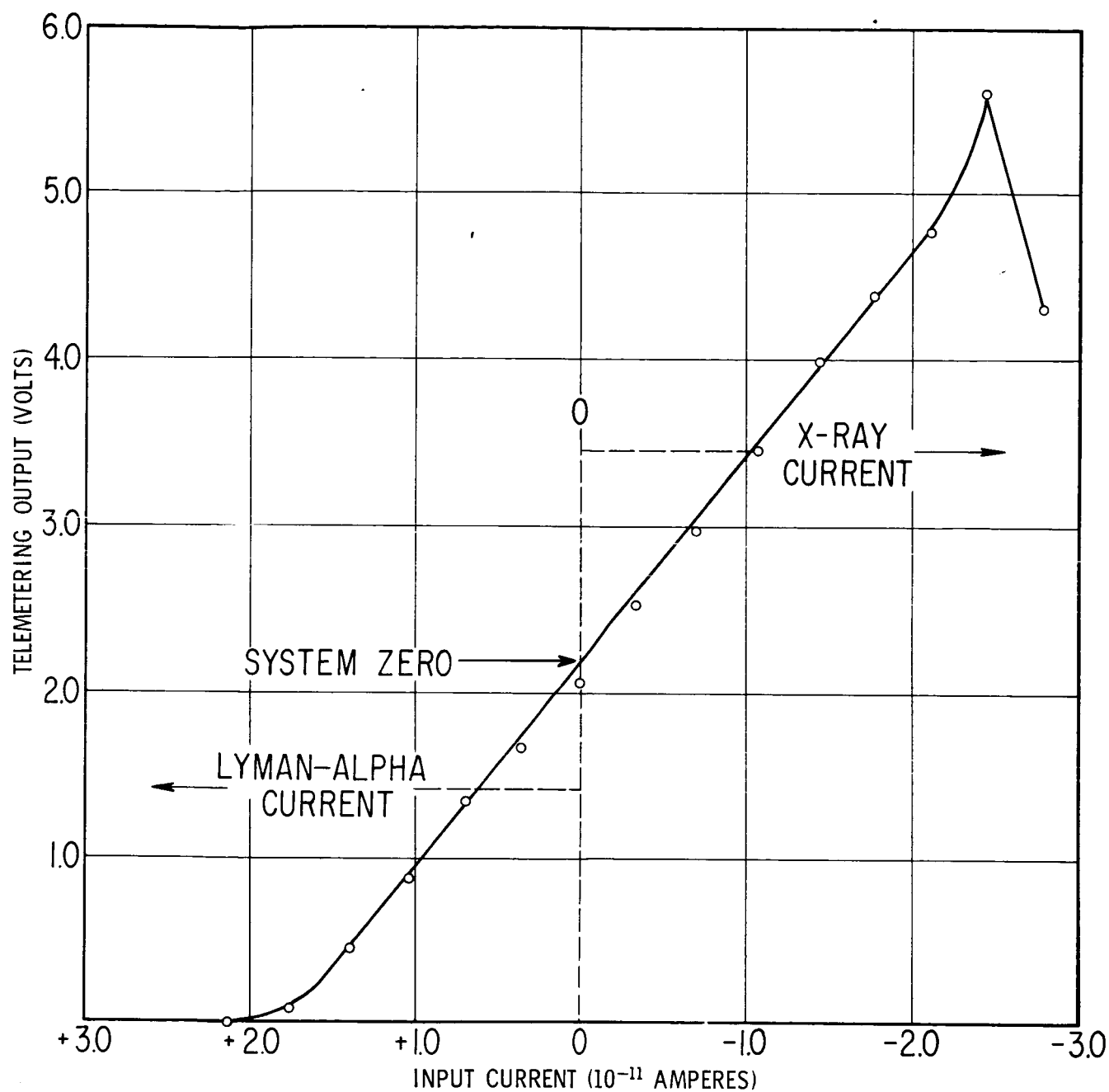from a cobalt-60 source

Figure 9 - Calibration curve for the Lyman-alpha and X-ray sensors;
ionization current as a function of telemetered voltage

The final step in the reduction of Lyman-alpha data is to take the Lyman-alpha sensor current (Figure 9) and obtain the correction factor for pitch angle by using Figures 10 and 11B. The corrected detector current is then divided by the Lyman-alpha detector sensitivity at 1216A of $1.74 \times 10^{-12}$ amp/erg cm$^{-2}$ sec$^{-1}$ to obtain Lyman-alpha radiation in ergs/cm$^2$/sec.

*Remarks*

Owing to Van Allen Radiation Belt electrons with energies above 150 kev, the detectors have been saturating most of the time. It is the opinion of the experimenters that only unsaturated detector data can be reduced and interpreted adequately by the previously described procedures. As an aid in interpreting the results that may be obtained, typical waveforms that may be found are illustrated in Figure 12.

Heavy Primary Cosmic Ray Experiment

The Heavy Primary Cosmic Ray Experiment employs a pulsed ionization chamber which is essentially cylindrical, 11 cm in diameter and 18 cm in length, and filled with argon gas at 9 atmospheres pressure. The output of this chamber is analyzed by means of a three-channel pulse-height analyzer. For a particle path length within the chamber of 7 cm, the respective outputs of the three channels correspond to relativistic primaries with atomic number Z greater than or equal to that of carbon, of fluorine, and of sulfur. These are therefore designated the C, F, and S channels. The output of the S channel is fed into a scaler with a scale of 2, while the outputs of the C and F channels are each fed into scalers with scales of 4. Each scaler output in turn activates an individual storage unit. The output of each such storage unit is a voltage which takes on integral values between 0 and 5 volts inclusive. When a storage-unit output is smaller than 5 volts, it increases by unity whenever the unit receives a pulse from its associated scaler. When the output is 5 volts, the next pulse returns the output voltage to zero. Because the counting rate of the heavy particles is slow, a long continuous pass is required to evaluate properly the number of ions detected.

The data from the Heavy Primary Cosmic Ray Experiment are sent on segments 4, 6, and 8 of the 960-cps subcarrier (see Figures 3 and 4) which is frequency-modulated
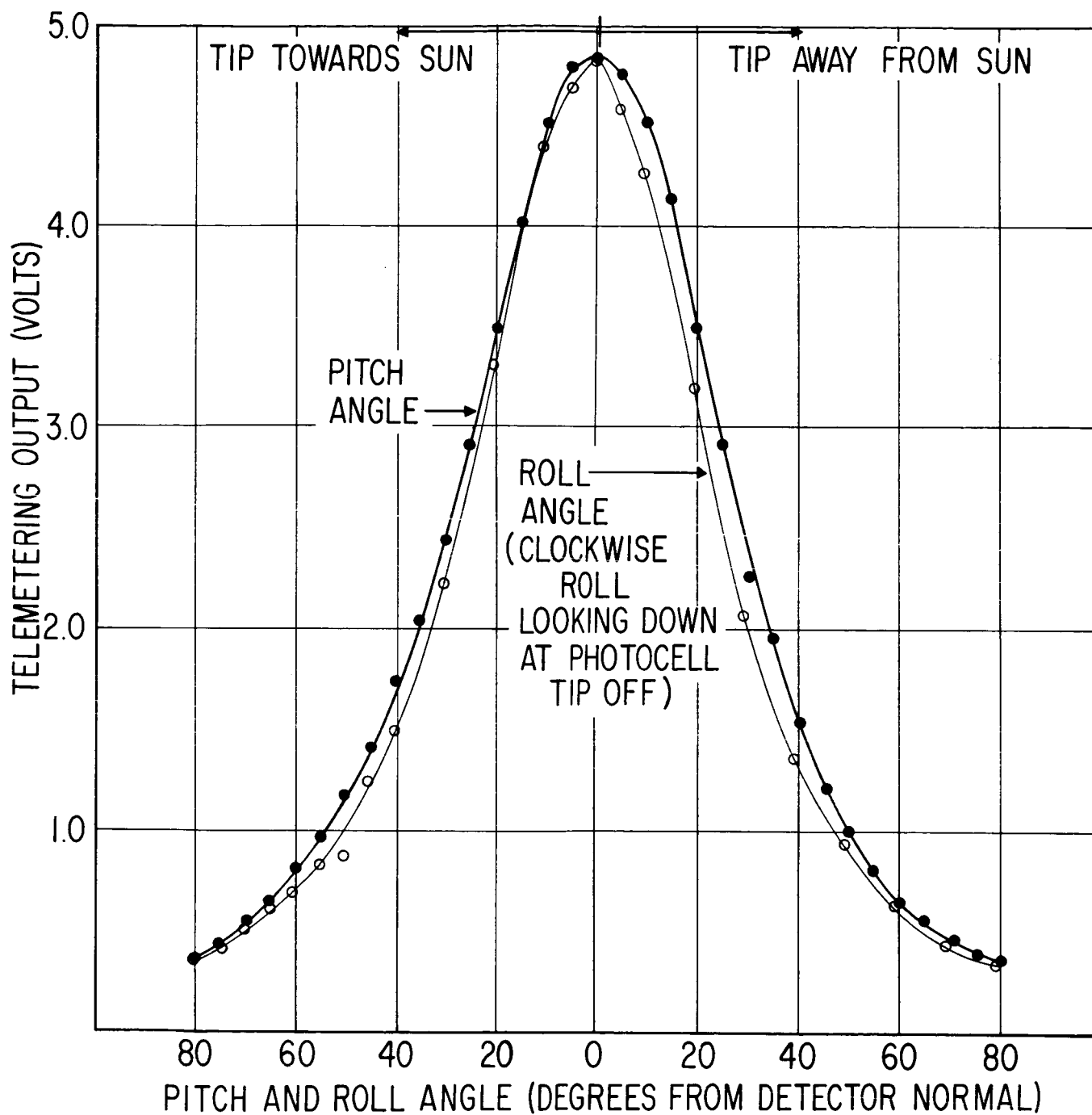
Figure 10 - Calibration curve for the solar aspect sensor; angle between the sensor axis and the direction to the sun (pitch angle)
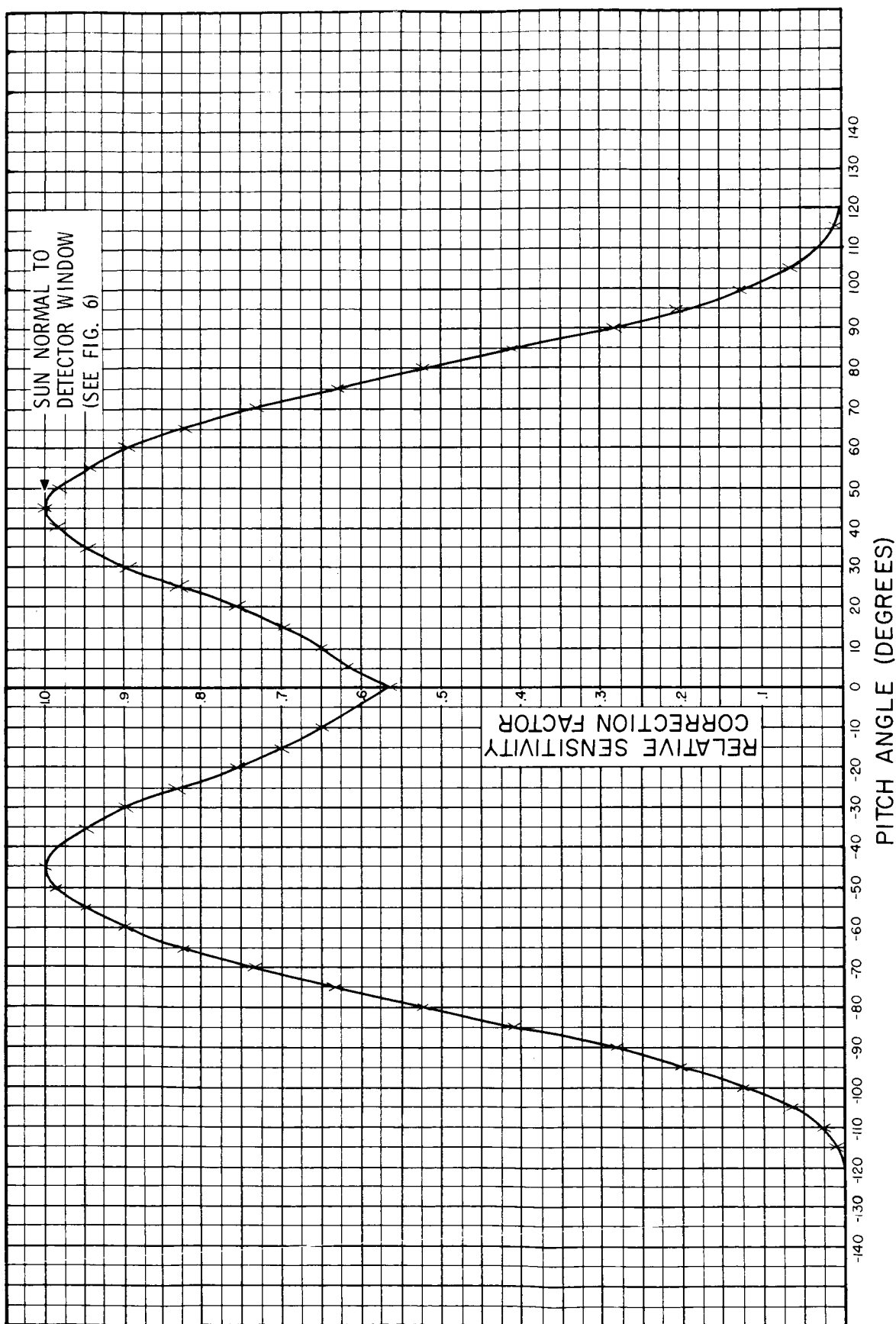
Figure 11A - Relative sensitivity correction factor of the X-ray detector system as a function of the pitch angle between the sun and the satellite equator
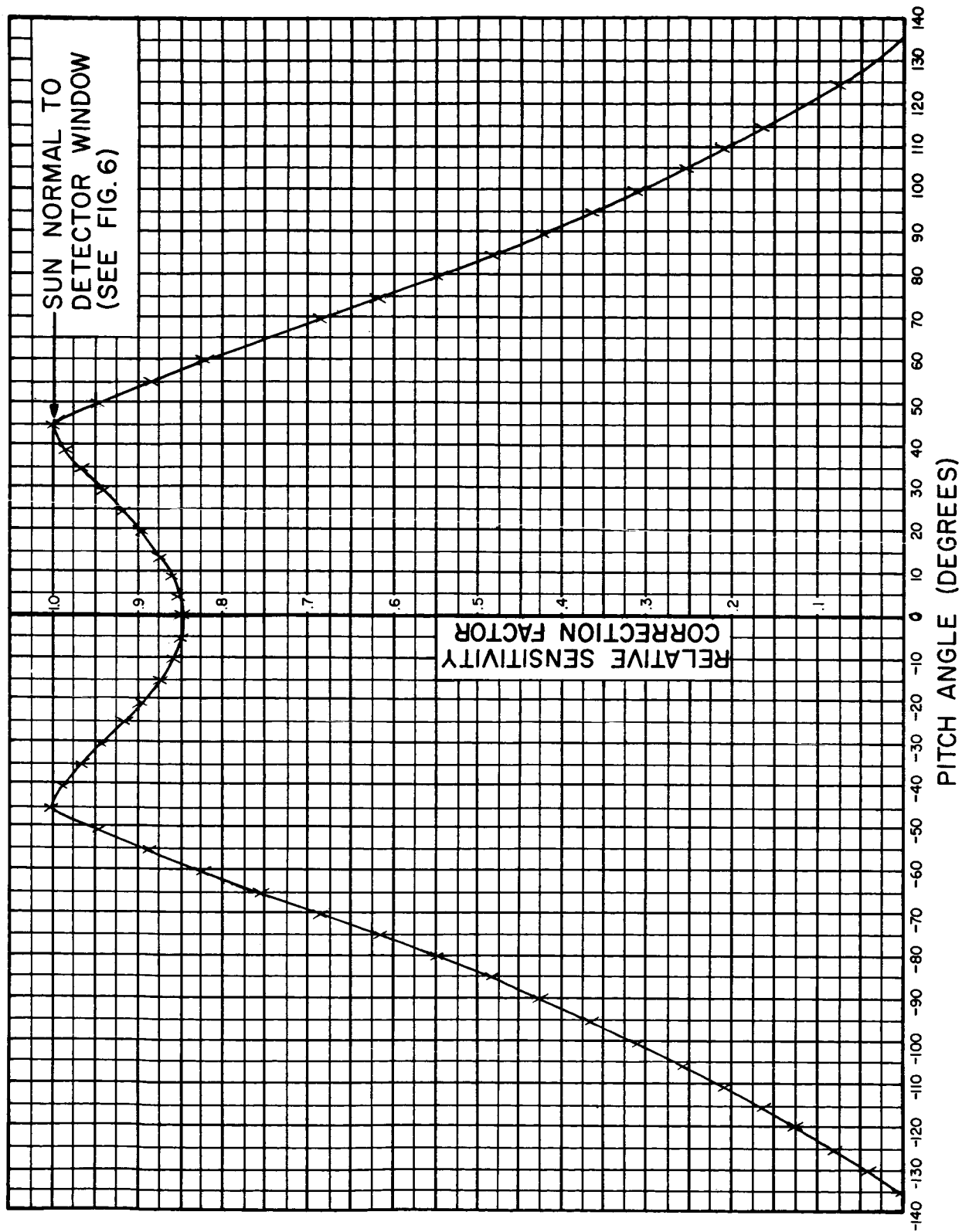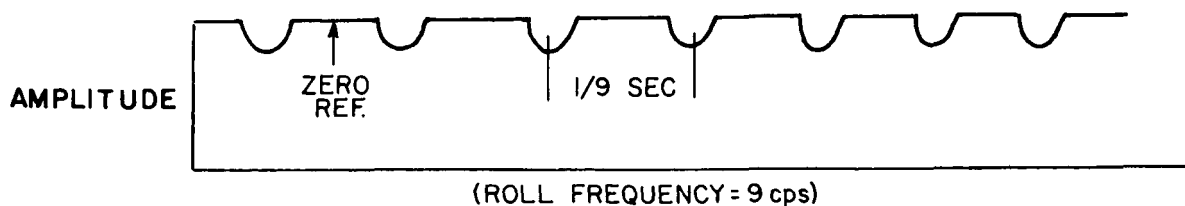
Figure 11B - Relative sensitivity correction factor of the Lyman-alpha detector system as a function of the pitch angle between the sun and the satellite equator

Type A - In sunlight and in regions of little X-ray radiation the
expected Lyman-alpha and X-ray signal shape is:

AMPLITUDE | ZERO REF. | 1/9 SEC

(ROLL FREQUENCY = 9 cps)

Type B - During unusual solar activity the signal will also have X-ray
data and should appear:

1/7 SEC

AMPLITUDE | ZERO REF. | 1/9 SEC

(X-RAY SIGNAL IS POSITIVE)
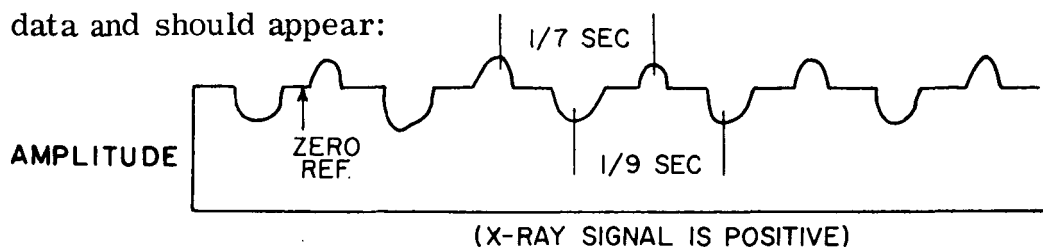
Type C - When the instrument is in regions of high radiation in the Van
Allen radiation belt, the X-ray data may be expected to have twice the fre-
quency of that from the sun:

1/14 SEC

AMPLITUDE | ZERO REF. | 1/9 SEC
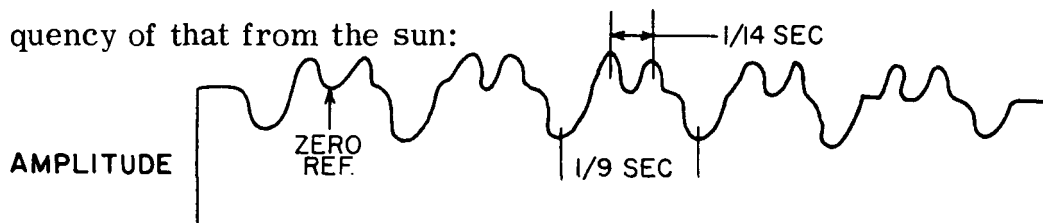
The X-ray signal produced by the Van Allen radiation belt may not
be phased as shown and may even tend to cancel the Lyman-alpha
signal. The Zero reference may shift upwards.

Type D - When the instrument is in darkness and not in a radiation area
no roll modulation will be seen and the shape will be:

AMPLITUDE | ZERO REF.

Figure 12 - Typical waveforms that may be obtained on the
Lyman-alpha and X-ray records

Type E - The X-ray detector also measures particle radiation from auroral activity and the Van Allen belts. At night this signal would appear:

AMPLITUDE

ZERO REF.
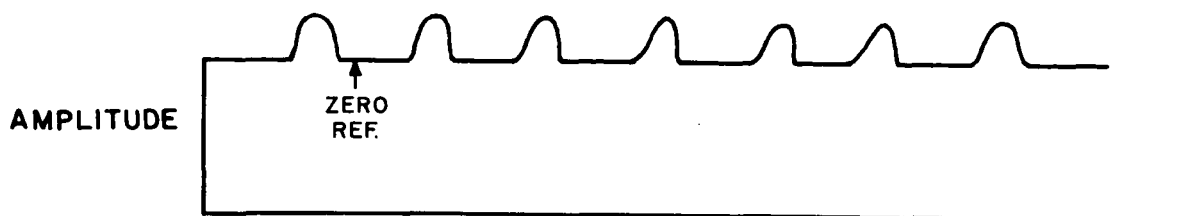
Type F - During night orbits above aurorae the data may have the following shape:

1/9 SEC

AMPLITUDE

ZERO REF.
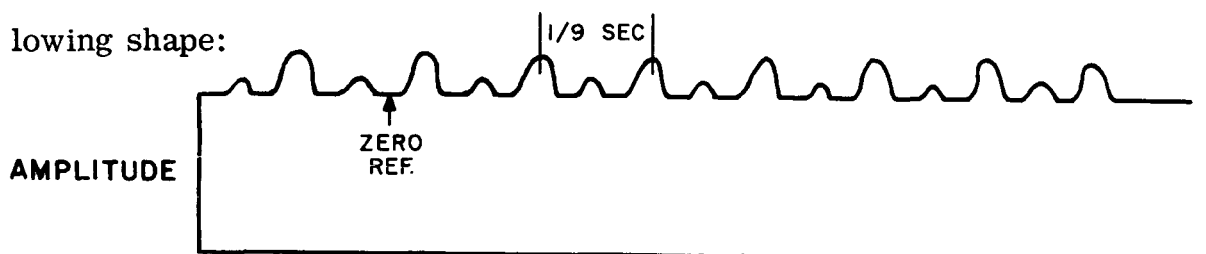
When the instrument is saturated, the signal will have one of the following four forms (H, I, J, K):

Type H - Saturated Condition:

APPROX. 5 V

AMPLITUDE
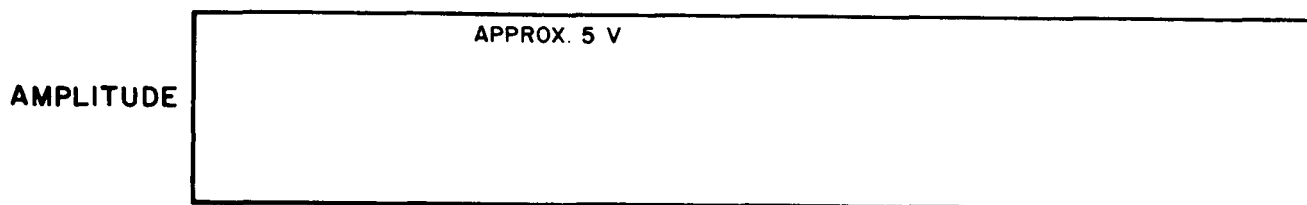
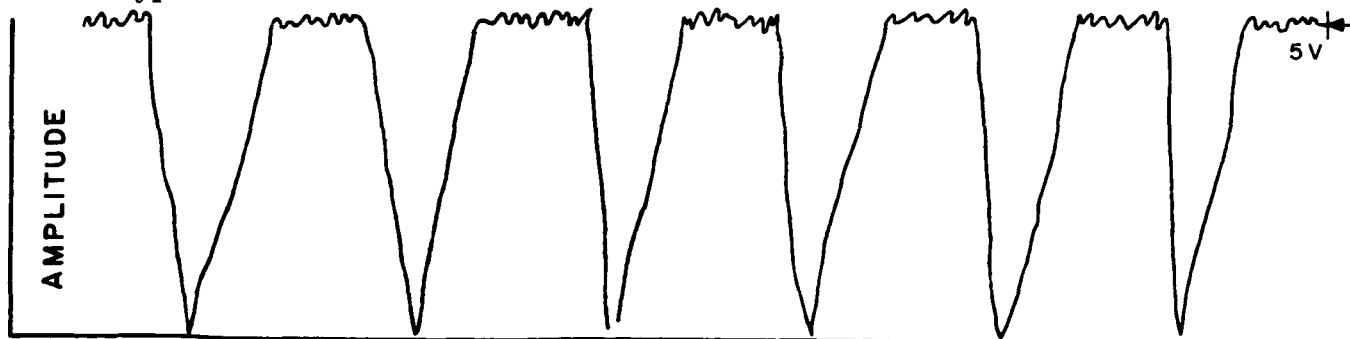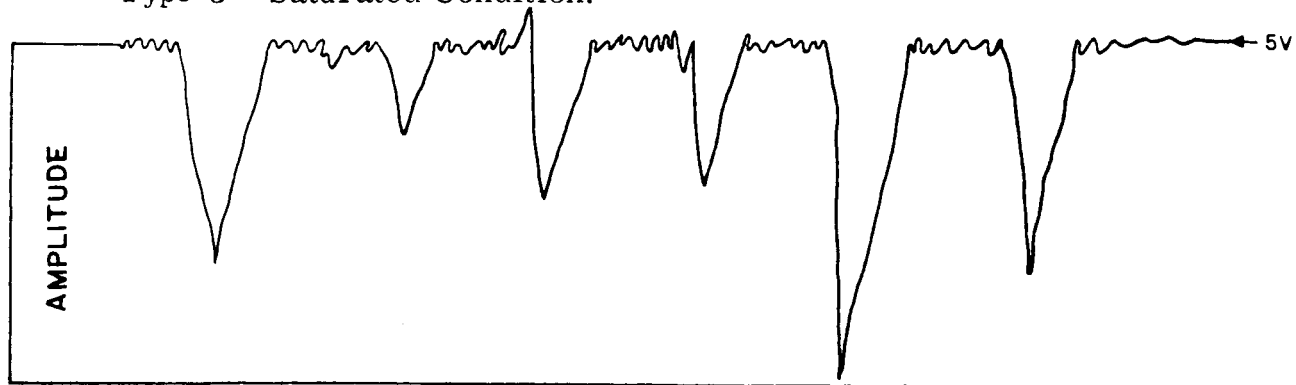Type I - Saturated Condition

5 V

AMPLITUDE

Figure 12 (Continued)

32

Type  J - Saturated Condition:
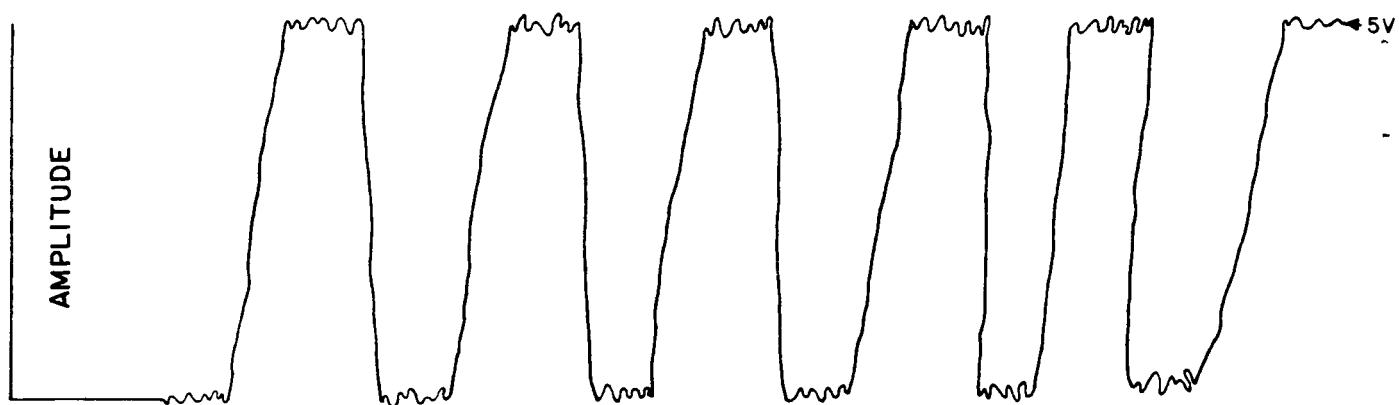
Type K - Saturated Condition:

Figure 12 (Continued)

with a maximum deviation of approximately 7.5 percent from the center frequency. Specifically, segment 4 corresponds to the S storage unit, segment 6 to the F storage unit, and segment 8 to the C storage unit.

Table 5 summarizes the information needed to obtain the counting rate of each of the segments. Note the anomalous pattern of the telemetered voltage for segment 8. Although the original pattern was the same as that for the other segments, a malfunction of the storage unit in the satellite has caused the pattern to change to the one shown. It is believed that useful data can still be obtained from this segment, since an analysis of the results obtained to date indicates that each unit change in voltage in the pattern shown in Table 5 still corresponds to 4 counts. However, all results from this segment should be carefully checked and should be regarded as less reliable than the results from the other segments. Recent experience indicates that on occasion the C storage unit returns to its original mode.

Table 5
Telemetry code for the Heavy Primary Cosmic Ray Experiment

| Particle Size | Segment | Counts per Volt | Voltage Pattern |
|---|---|---|---|
| $Z \geq 16$ | 4 | 2 | 0,1,2,3,4,5,0,1, etc. |
| $Z \geq 9$ | 6 | 4 | 0,1,2,3,4,5,0,1, etc. |
| $Z \geq 6$ | 8 | 4 | 3,4,5,4,5,3,4,5, etc. |

Segments on 960-cps subcarrier

1  5.5-volt Reference
2  0-volt Reference
3  Lyman-alpha and X-ray
4  Heavy Primary Cosmic Ray Experiment $\geq 16$
5  Lyman-alpha and X-ray
6  Heavy Primary Cosmic Ray Experiment $\geq 9$
7  Solar Aspect
8  Heavy Primary Cosmic Ray Experiment $\geq 6$
9  Exposed Solar Cell
10  Solar Cells and Nickel-Cadmium Batteries
     (Monitored Power Supply)

## Exposed Solar Cell Experiment

The Exposed Solar Cell Experiment is intended to study the effects of micrometeorites and radiation upon exposed solar cells. Ten Hoffman 120c solar cells, in series with a 100-ohm resistive load across the output, are located on the satellite equator, completely unprotected and exposed to the space environment. The effects of this environment on solar cell performance can be determined by measuring the voltage output as a function of time in orbit, and comparing later outputs with the initial output. Because the voltage of the solar cell also varies with its aspect relative to the sun, it is necessary to utilize the solar aspect data to determine the angle of incidence of the solar radiation.

The solar cell experiment appears on segment 9 of the 960-cps subcarrier. The maximum output voltage of the cell is determined by measuring the value of the peaks of the waveforms (waveforms due to satellite spin relative to the sun) and relating these measurements to voltage through the 0-volt and 5.5-volt references. This measured voltage output and the solar aspect data may be used along with Figure 13 (a preflight calibration of the solar cell output as a function of solar incidence angle) to estimate solar cell performance.

## Battery Performance Experiment

The power supply is monitored by a telemetered gage voltage on segment 10 of the 960-cps subcarrier. This gage voltage is based on the battery charge received from a patch of two parallel patches of 34 Hoffman 52c solar cells located on the solar cell panels. The monitored nickel-cadmium batteries are designed to have a nominal voltage of 10.4 volts (range 9.8 and 11.8 volts) and function to supply the multiplexer and voltage converter.

The actual voltage of the batteries can be determined by first measuring the deflections of the tenth segment on the 960-cps telemetered record and converting these deflections to telemetered voltage by use of the 0-volt and the 5.5-volt reference deflections. Next the telemetered voltages can be used along with Figure 14 to obtain the actual battery voltage.
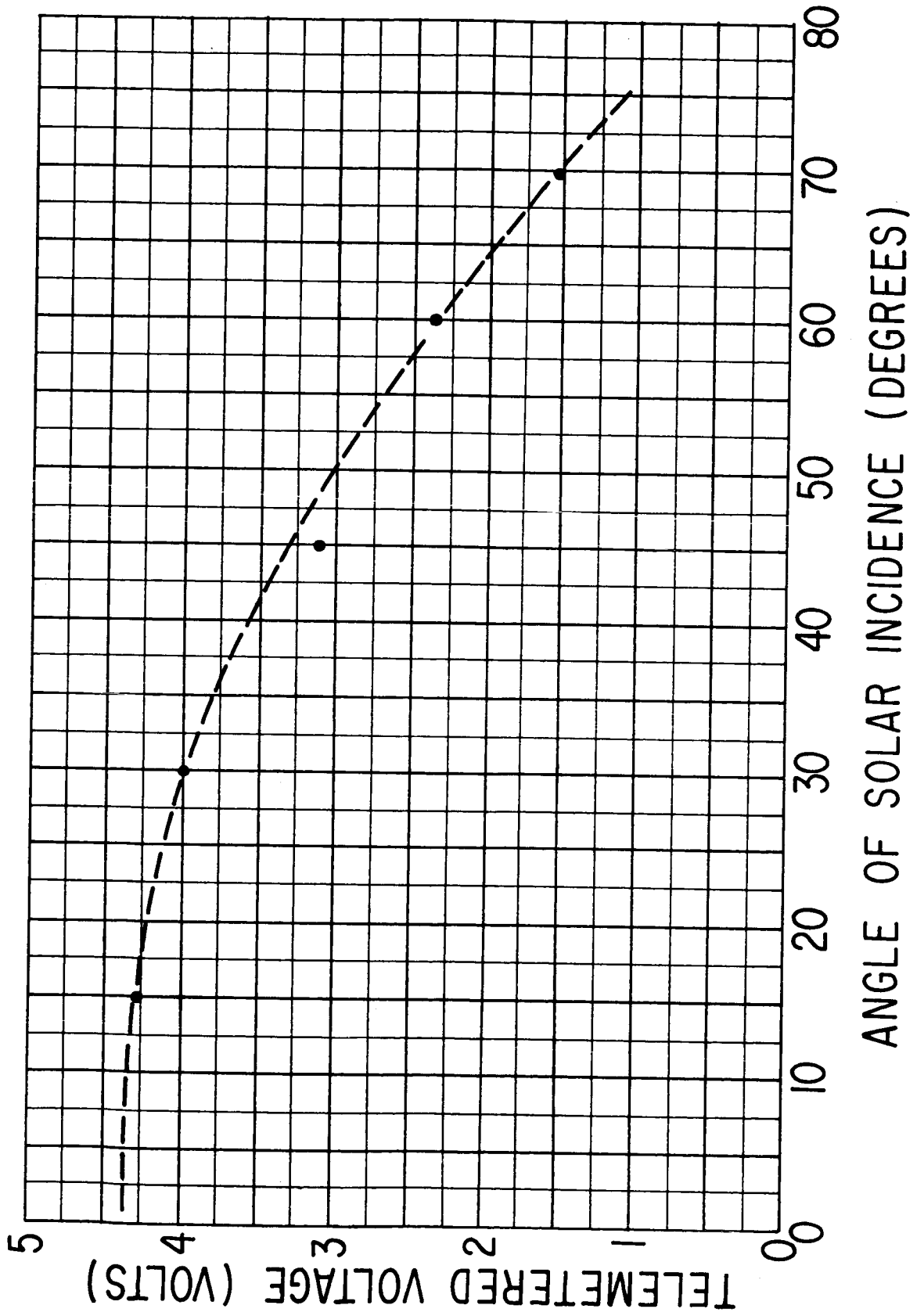
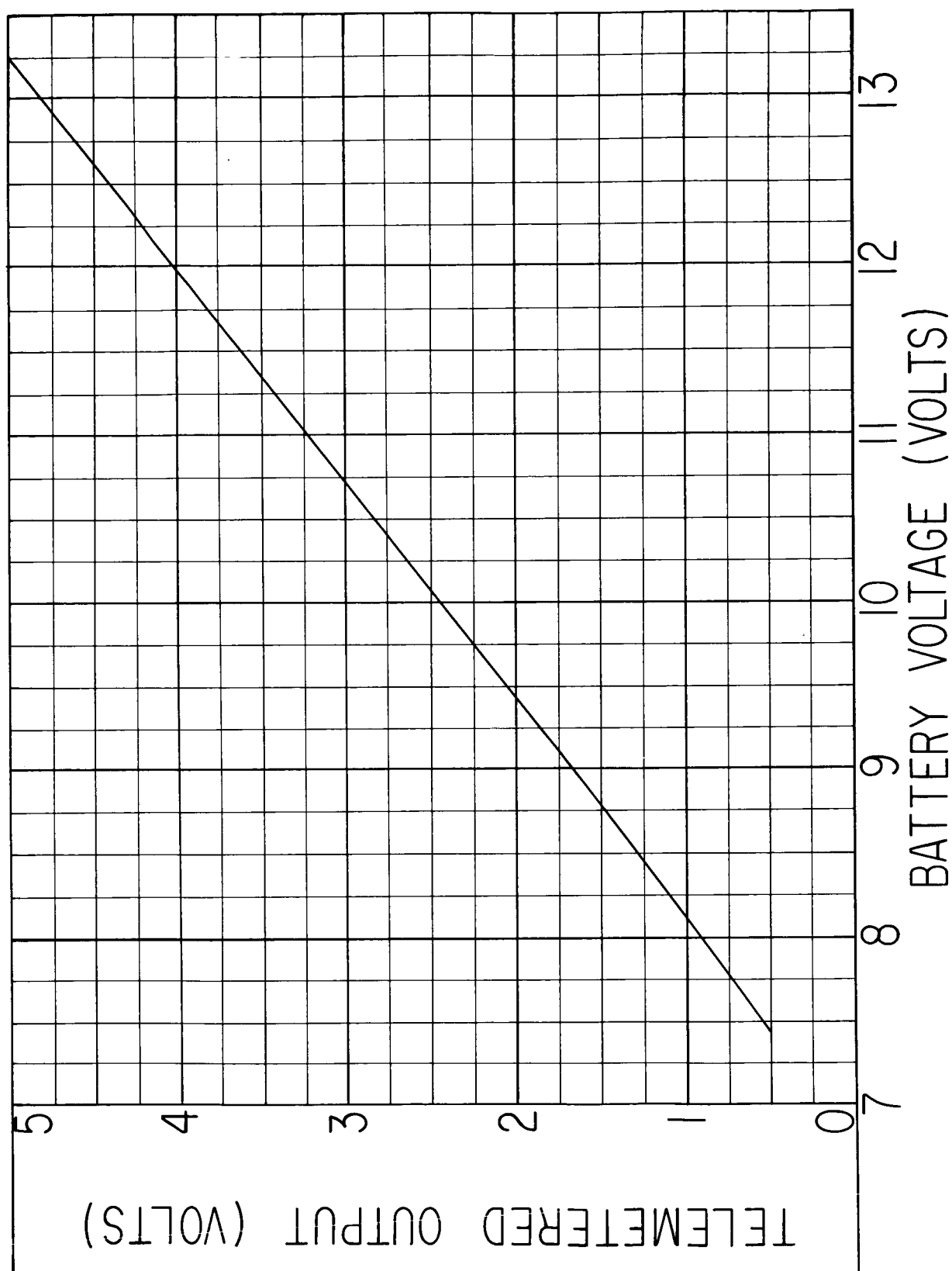Figure 13 - Variation of solar cell output as a function of solar incidence angle

Figure 14 - Variation of telemetered voltage as a function of
actual solar cell and battery voltage

One significance of the monitored battery voltage is that it indicates any deterioration of the power supply system. It has been noted that when the battery voltage is low, the Lyman-alpha X-ray experiment telemetered signal will appear on all segments of the 960-cps subcarrier.

## 1300-CPS SUBCARRIER CORPUSCULAR RADIATION EXPERIMENT

### General Description

The 1300-cps subcarrier is used only to telemeter data from the Total Cosmic Ray, or Corpuscular Radiation Experiment, which is designed for comprehensive spatial and temporal monitoring of total cosmic ray intensity, geomagnetically trapped corpuscular radiation, and solar protons.

The instrumentation for this experiment is shown schematically in the block diagrams of Figure 15. Two Geiger-Mueller counters are used: a small one (Anton type 302) associated with a large scaling factor which is "on scale" in the presence of the highest expected intensity in the radiation belts, and a larger counter (Anton type 112) used with a smaller scaling factor which is useful in the range from cosmic ray intensity to an intermediate level. Over the portion of the dynamic range in which the counters overlap an absorption coefficient can be determined, since the counters are covered by different but known thicknesses of absorber.

The output voltages of the two Geiger-Mueller counter channels frequency-modulate the 1300-cps subcarrier oscillator. This oscillator has four discrete frequency "states," as determined by the combination of the two scaler output voltages. Each of these four states corresponds to a unique combination of the two states of the final stages of the two scaling circuits as indicated in Table 6 and illustrated in Figure 16. The frequencies listed in Table 6 may vary slightly as the temperature of the instrumentation varies. They are typical of those observed during the first two months of orbital flight. A change in state of the 112 counter scaler causes a change in subcarrier frequency of 40 to 60 cps, while a change in state of the 302 counter scaler causes approximately a 90-cps frequency shift. Therefore, the two scaler outputs are readily distinguished even when the absolute frequencies are not measured.
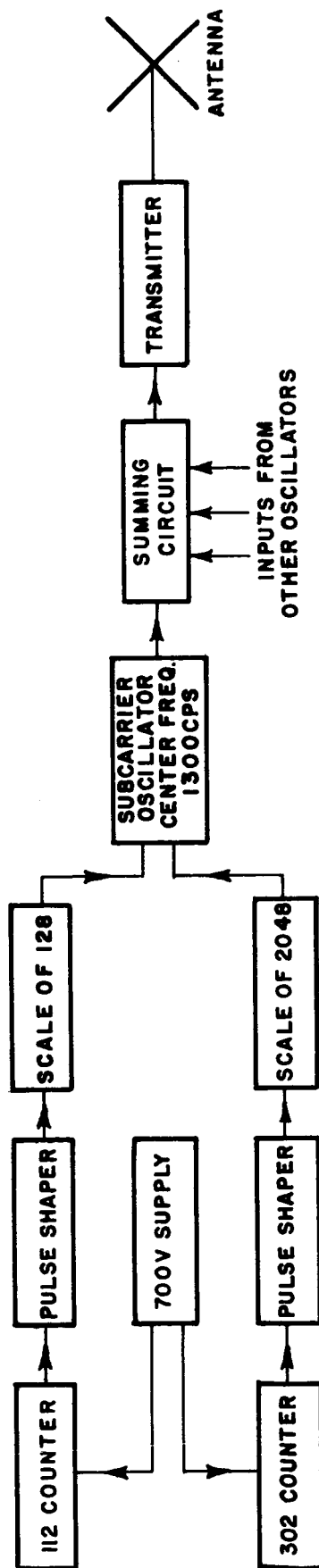
Figure 15 - Block diagram of the Total Cosmic Ray Experiment

Table 6
Telemetry code for the Total Cosmic Ray Experiment

| State | SCO frequency (cps) | 112 counter scaler condition | 302 counter scaler condition |
|-------|---------------------|------------------------------|------------------------------|
| 1 | 1219 | off | off |
| 2 | 1256 | on | off |
| 3 | 1304 | off | on |
| 4 | 1368 | on | on |

## Detector Characteristics

Both Geiger-Mueller counters are halogen-quenched and have an essentially unlimited operating lifetime. The temperature of the detector assembly on the satellite has been thus far within the range -20° to 80°C which is well within the operating range of the counters and associated circuits.

The characteristics and dimensions of the counters are indicated in Table 7, and a summary of the absorbers surrounding the counters is given in Table 8. The omnidirectional flux $J_0$ is

$$J_0 = \frac{R}{\epsilon G_0} ,$$

where $\epsilon$ and $G_0$ are listed in Table 6 and R is the "true counting rate," defined as the counting rate of a counter and scaler having zero dead time but with otherwise identical characteristics. The instrumentation was calibrated with an X-ray source before flight

Table 7
Geiger-Mueller Counter Characteristics

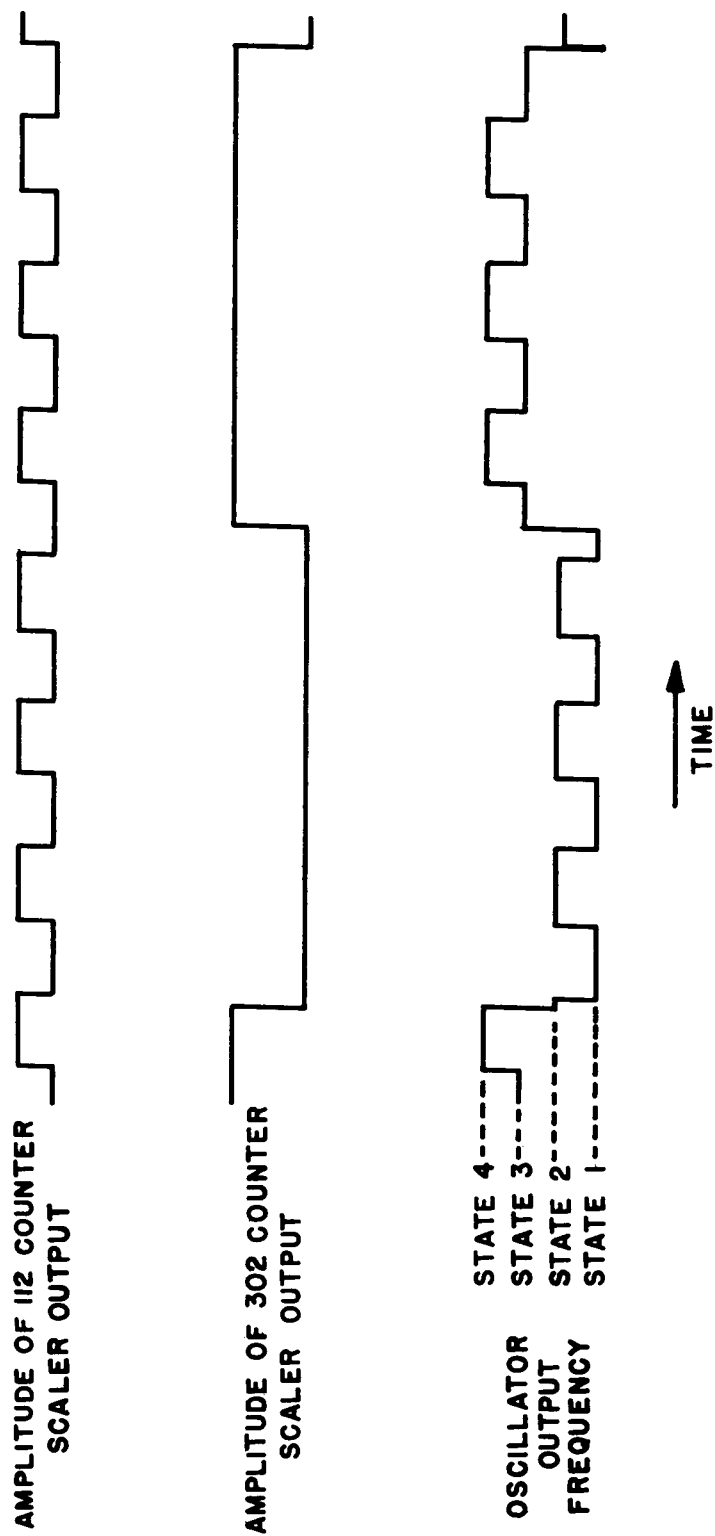| Characteristics | 112 counter | 302 counter |
|-----------------|-------------|-------------|
| Effective diameter a (cm) | 1.82 ± 0.01 | 0.65 ± 0.03 |
| Effective length $\ell$ (cm) | 5.27 ± 0.1 | 0.94 ± 0.1 |
| Omnidirectional geometric factor $G_0$ (cm$^2$) | 9.02 ± 0.19 | 0.61 ± 0.09 |
| Absolute efficiency $\epsilon$ for energetic charged particles | 0.81 ± 0.03 | 0.84 ± 0.05 |
| Omnidirectional flux $J_0$ for energetic charged particles | 0.137 $R_{112}$ | 1.95 $R_{302}$ |
| Scaling factor s | 128 | 2048 |

Figure 16 - Subcarrier output of the Total Cosmic Ray Experiment

Table 8
Absorbers used in the Geiger-Mueller Counters

| 112 counter | | | |
|---|---|---|---|
| Item | Material | Absorption $(mg/cm^2)$ | Solid Angle (steradians) |
| Counter cathode | $\begin{bmatrix} 28\% \text{ Cr} \\ 72\% \text{ Fe} \end{bmatrix}$ | 40 for 81% of cathode surface<br>241 for 19% of cathode surface | -- |
| Counter ends | Ceramic | 0.4 cm thick | -- |
| Absorber | Al | 260 ± 3 | $4\pi$ |
| Absorber | Pb | 1150 ± 30 | $4\pi$ |
| Detector box | Mg | 140 ± 40 | $4\pi$ |
| Payload structure | Mostly Al | >1700 | 3.9 |
| Instrument column | Mostly Al | >3000 | 0.84 |
| 302 counter | | | |
| Counter wall | $\begin{bmatrix} 28\% \text{ Cr} \\ 72\% \text{ Fe} \end{bmatrix}$ | 402 ± 20 | * |
| Detector box | Mg | 140 ± 40 | 4 |
| Payload structure | Mostly Al | >1700 | 3.9 |
| Instrument column | Mostly Al | >3000 | 0.84 |

*The section of the counter wall having this absorption is 0.57 cm long. The remainder of the wall and the ends are a combination of stainless steel, ceramic, and aluminum, having several times this absorption.

to ascertain the relation between r, the apparent counting rate, and R. The data are accurately represented by the semi-empirical expressions listed in Table 9, where the values of $\tau$ are correct at 23°C and at the nominal primary power supply voltage (6.5 volts). These values of $\tau$ vary somewhat with temperature and supply voltage; the effect is to change the curves by an amount that increases as R increases. For the 112 counter at R = 2,000 counts/sec the temperature coefficient of r is about + 1.5%/°C and its supply voltage coefficient is about + 1.7% for a 1% change in supply voltage. The temperature and the supply voltage are expected to be always within the ranges -30° to 80°C and 5.8 to 7.2 volts, respectively. Comparable data for the 302 counter are not available, but are

Table 9
Conversion from true rate R to apparent rate r

| Counter Channel | Range of Applicability | Formula | $\tau_1$ (sec) | $\tau_2$ (sec) |
|---|---|---|---|---|
| 112 | R = 0 to 5,000 sec$^{-1}$ | $r = \dfrac{R}{1 + R\tau_1}$ | $7.30 \times 10^{-4}$ | -- |
| 112 | R = 4,000 to 20,000 | $r = \dfrac{R}{1 + R\tau_1}\, e^{-R\tau_2}$ | $5.04 \times 10^{-4}$ | $6.2 \times 10^{-5}$ |
| 302 | R = 0 to 100,000 | $r = \dfrac{R}{1 + R\tau_1}$ | $3.64 \times 10^{-5}$ | -- |
| 302 | R > 100,000 | R is not expected to exceed 100,000 | | |

believed to be similar to those for the 112 counter. The value of r is obtained from the telemetry records and is simply

$$r = \frac{ns}{t(n)} \, ,$$

where s is the scaling factor and t(n) is the time for n full cycles of the scaler output waveform. It should be noted that the relation between R and r is a double-valued function. It is expected that the counting rate of the 302 counter will always remain on the ascending portion of the curve. The ambiguity of the 112 counter curve can nearly always be resolved by the use of auxiliary data — the spatial dependence of the counting rate, the simultaneous rate of the 302, and the statistical fluctuations of the 112 rate. It should be further noted that the values of $J_0$ given in Table 7 are meaningful only if all counts are produced by energetic particles passing directly through the counters. Other detection processes require a different relation between $J_0$ and R. If, for example, the counts are due only to the bremsstrahlung from 60-kev electrons stopped in the walls of the equipment:

$$J_0 = (4 \times 10^5)\, R_{302} \ .$$

Timing Records

The importance of recording accurate and reliable time on all magnetic tapes and oscillograph records cannot be overstressed. The orbital information is obtained as a function of time. Therefore, the time correlation of all data is necessary in order to

establish the correspondence between a particular bit of data and the satellite location of time of receipt of that data. If this correspondence cannot be established the data are usually worthless. A time base must be recorded on recordings at the time of signal reception. A local voice announcement of the time, or a manually applied mark on the records, has not proven satisfactory. By far the simplest and most practical system is to record the output of a WWV or other standard time signal receiver on a second channel of the recordings (Figure 17). All recordings should include an absolute time announcement by the standard time station. Then, if care is taken to record the universal date on the records, the time information is complete and unambiguous.
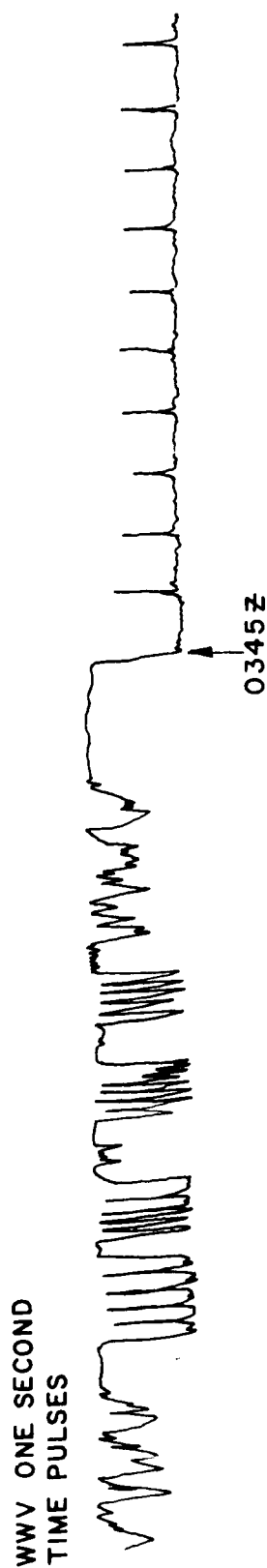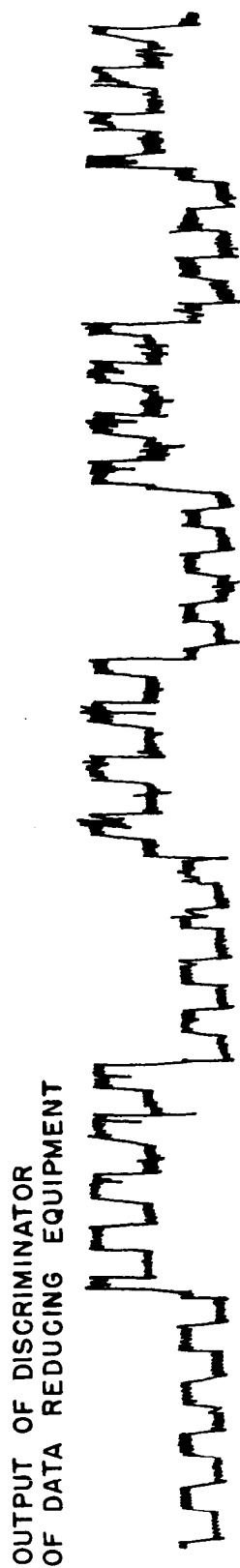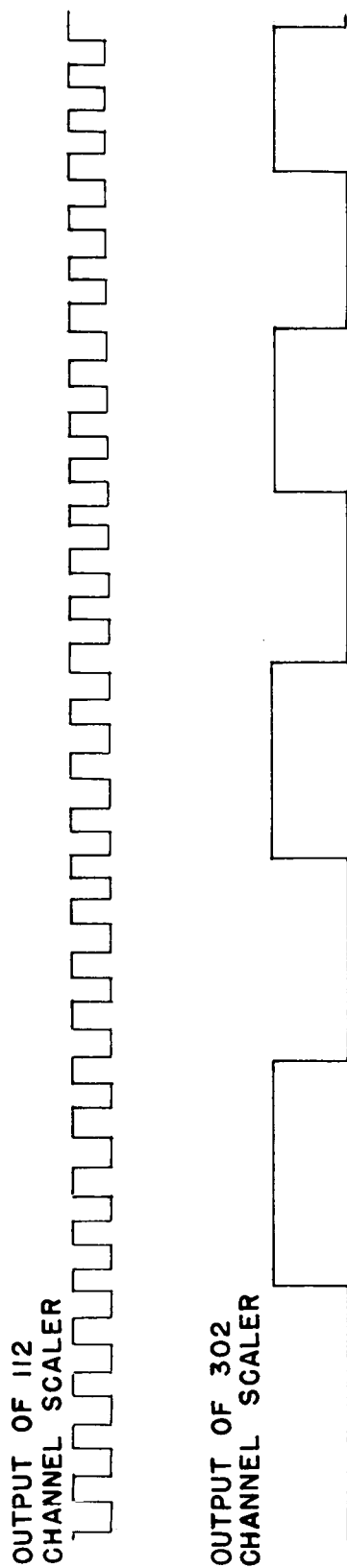
Data Reading

The output of the FM discriminator on the ground is, in the absence of noise, of the same form as the subcarrier oscillator output illustrated in Figure 16. Noise makes the waveform more difficult to read, but since it is a composite of two rectangular waveforms, good discrimination against noise spikes can be made by a trained data reader. Samples of actual recordings are shown in Figures 17A, 17B, 17C, and 17D along with their interpretations, to illustrate the method of reading the data.

In Figure 17A the ratio of 112 to 302 scaler output switching rates is 7.4 and the signal-to-noise ratio is large. Under these conditions the data are easily readable. This record also illustrates the manner in which the WWV time signal is recorded on the oscillograph records. A coded time announcement is shown followed by the 1-second markers. In Figure 17B the scaler output ratio is somewhat lower (2.6), and in Figure 17C it is nearly unity (1.03). In both cases the data are still easily readable. Note that in Figures 17A and 17B the rates change appreciably during the 25-second intervals.

Figure 17D shows the appearance of the data in the presence of considerably more noise. In this recording segment no switching of the 302 scaler output is observed. The 112 rate can be determined reasonably well.

# CONCLUDING REMARKS

A description of the experiments, the detector calibrations the telemetry codes, samples of actual data recordings, and other pertinent information for the 19.992-Mc

OUTPUT OF 112
CHANNEL SCALER

OUTPUT OF 302
CHANNEL SCALER

OUTPUT OF DISCRIMINATOR
OF DATA REDUCING EQUIPMENT
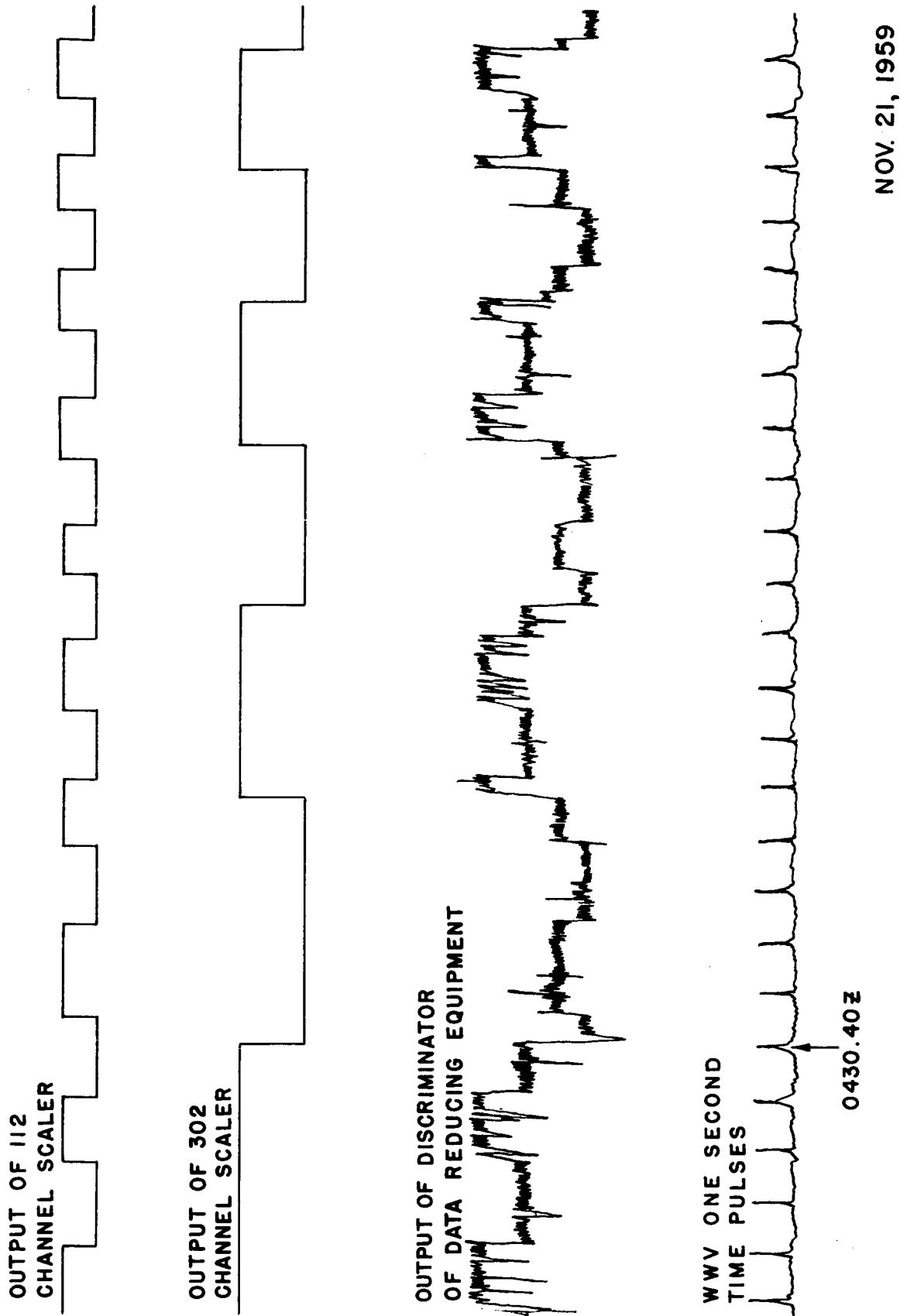
WWV ONE SECOND
TIME PULSES

0345 Ƶ

NOV. 21, 1959

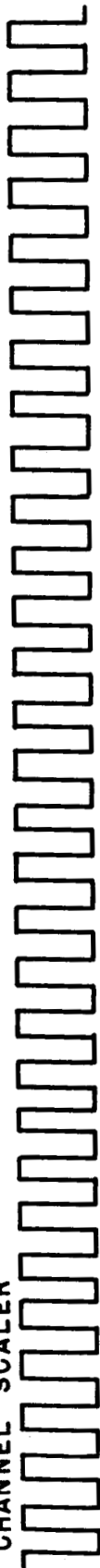Figure 17A - Actual recordings from the Total Cosmic Ray Experiment

OUTPUT OF 112
CHANNEL SCALER

OUTPUT OF 302
CHANNEL SCALER

OUTPUT OF DISCRIMINATOR
OF DATA REDUCING EQUIPMENT

WWV ONE SECOND
TIME PULSES

0430.40 ̄z

NOV. 21, 1959

Figure 17B - Actual recordings from the Total Cosmic Ray Experiment
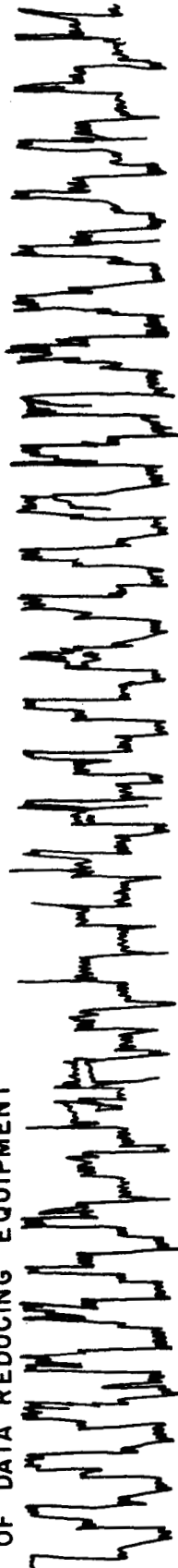
OUTPUT OF 112
CHANNEL SCALER

OUTPUT OF 302
CHANNEL SCALER

OUTPUT OF DISCRIMINATOR
OF DATA REDUCING EQUIPMENT

WWV ONE SECOND
TIME PULSES

0432.15ᶻ

NOV. 21, 1959 ᶻ

Figure 17C - Actual recordings from the Total Cosmic Ray Experiment

OUTPUT OF 112
CHANNEL SCALER

OUTPUT OF 302
CHANNEL SCALER

OUTPUT OF DISCRIMINATOR
OF DATA REDUCING EQUIPMENT

WWV ONE SECOND
TIME PULSES

0644.15ᵶ

NOV. 15, 1959 Z

Figure 17D - Actual recordings from the Total Cosmic Ray Experiment

48

transmitter of Satellite 1959 Iota have been presented herein. This information is sufficient for the recording and preliminary analysis of telemetered data. Some additional information relating to 1959 Iota is also available in the open literature listed in the bibliography.

# BIBLIOGRAPHY

International Geophysical Year Bulletin No. 29, November 1959

"Reports on Radiation Belts," Science News Letter 77(7):101, 13 February 1960

"Meteors Little Threat to Short Space Trips," Science News Letter 77(7):105, 13 February 1960

Klass, P. J., "Explorer VII Reports Sporadic Radiation," Aviation Week 72(2):29-30, 11 January 1960

Ludwig, G. H., and Whelpley, W. A., "Corpuscular Radiation Experiment of Satellite 1959 Iota (Explorer VII)," Journal of Geophysical Research 65:1119-1124, April 1960

Kupperian, J. E. Jr., and Kreplin, R. W., "Optical Aspect System for Rockets," Review of Scientific Instruments 28(1):14-19, January 1957

Annals of the International Geophysical Year VI:331-340, 1957-1958